ISVR
University of Southampton

Internship 2013

Numerically solving the sound transmission in the intake of a turbofan engine with non-axisymmetric lining

Author:
Joost Maas

Supervisors:
Prof. Jeremy Astley
Dr. Rie Sugimoto

January 21, 2014

Contents

1 Acknowledgements

This report is the result of a period of three and a half months, from September 2 to December 20, 2013, during which I fulfilled an internship at the Institute for Sound and Vibration (ISVR) at the University of Southampton, U.K. The internship is part of the master degree in Engineering Fluid Dynamics at the University of Twente, the Netherlands, which I will be finishing after returning back to the Netherlands.

The internship at the ISVR gave me a chance to peek into the world of the many PhD projects in the Rolls-Royce University Technology Centre in Gas Turbine Noice, to which I am very grateful. It's a world formerly unknown to me and I consider the experience of working in the University Technology Centre alongside the PhD students who have worked or will work here for multiple years on a variety of subjects a valuable lesson which will help me a lot in deciding what to do after finishing the master degree.

For all of this and more, I most of all thank my two supervisors, Professor Jeremy Astley and Dr Rie Sugimoto, who have taken such good care of me during my time here. Not only during meetings and discussions on the assignment, for which they always seemed to be available when necessary, but also outside of the office, helping me get started in this city I had never visited before and giving tips on things not to miss in my spare time.

I experienced great joy in puzzeling for the right answers to the problems I faced in the assignment. The subject of turbofan noise is one I had not worked on so far but it is definitely one I will keep in mind for the future. I hope I have been able to contribute even a tiny bit to the many great research projects that the ISVR is working on and who knows, they might see me back one day.

Joost Maas
December 20, 2013

2 Introduction

Background

Analysis and consequently reduction of airplane noise is becoming more important as requirements and regulations on the subject of airplane noise become more severe. In modern airplane turbofan engine design, sound reduction focuses for a big part on fan noise sources, as these are the main contributors to modern high bypass ratio turbofan engine noise. Furthermore, the two main fan noise sources can be devided in 'rotor-alone' and 'rotor-stator interaction' tones. Rotor-alone tones are the principal fan noise sources at supersonic fan speeds and exists due to the steady pressure field attached to the supersonic duct fan. Rotor-stator interaction is the principal noise source at subsonic speed and exists due to rotor blade wakes impinging on fixed stator vanes. In fan noise analysis, the emphasis will be on rotor-alone noise sources.

An important approach in reducing fan noise in turbofan engines is the use of acoustic lining of the intake duct of the fan. This acoustic lining, used in almost every commercial airplane engine today, attenuates the noise emmited from fan sources. Most of the current commercial airplane engines use splices in order to attach the lining: thin strips joining together the lining panels on the duct wall parallel to the duct axis. These strips are made of 'acoustically hard' material, meaning they reflect and scatter incident noise modes, rather then to absorp them as is the main purpose of the lining. In recent years, the use of spliceless liners has become more conventional, its first commercial use being the Rolls-Royce Trent 900 turbofan engine of the Airbus A380 airplane. The main advantage of the spliceless liner is the absence of the negative effect on the noise attentuation of the splices; disadvantages are found in the enhanced difficulty to install the spliceless liner and consequently the enhanced difficulty to repair or replace them in case of damages. Damages and repairs therefore result in small non-attenuating areas, modelled as acoustically hard patches, having the same acoustic disadvantages as liner splices.

One of the difficulties in analysing the radiated sound field from turbofan noise sources lies in computing the acoustic effects of these liner splices and patches. As their specific wall impedence differs greatly from the lining itself, they tend to make the lining non-axisymmetric and, as mentioned before, the fact that they are acoustically hard results in the scattering of incident acoustic modes into various different acoustic modes, some of them less well attenuated by the lining and therefore increasing the radiated sound field from the engine. Over the years, many different models and codes have been produced in order to overcome this difficulty. One of the most well known semi-analytical models is the one by Cargill [1], who uses Green's function methods in order to derive an integral expression for the scattered field as a results of the splice or patch. The Cargill code, however, has one major disadvantage in the fact that it needs the geometry of the duct to be represented as a uniform cylindrical duct, which in reality is hardly ever the case. More recent studies on modelling the scattering behaviour of non-axisymmetric lining emphasises full three dimensional computational methods using Finite Elements (FE) and Boundary Element (BE) models, which do not have the disadvantage of geometrical limitations.

The use of computational methods in the calculation of sound propagation has been investigated since the 1970's. In 1977, A. L. Abrahamson [2] proposed one of the earliest finite element formulations for sound propagation in axisymmetric ducts in the presence of a mean flow. In 1978, Astley and Eversman [3] proposed a finite element method for the sound transmission in non-uniform ducts and compared it with the method of weighted residuals as described by Eversman, Cook and Beckemeyer [4] and Vo and Eversman [5].

In 2003, McAlpine, Wright, Batard and Thezelais [6] presented results obtained with a finite element method on the scattering effect by liner splices. They used a 3D model of a cylindrical duct containing a uniform mean flow and neglected nonlinear effects. For the actual FE method, they used the program ACTRAN which enabled them to specify duct boundary conditions in terms of the modes in the duct and implement the effect of irrotationality of the flow. They conclude their model to give realistic solutions based on the way the acoustic energy is confined to the predicted scattered mode numbers and the model enables them to draw conclusions on the attenuation of the lined duct for different scattered modes. In 2007, Wright and McAlpine [7] wrote a short communication on the expension of the FE method which allowed the 3D, non-axisymmetric lined duct problem without flow to be formulated as a 2D Helmholtz eigenvalue problem, which is faster and computational less demanding than full 3D FE methods such as the ACTRAN code. The expension of the short communication allowes the 2D eigenvalue problem to be formulated for the non-axisymmetric duct problem in presence of a flow as well.

In 2006, Tester, Powles, Baker and Kempton [8] proposed an analytical model for the scattering of modes due to a acoustically hard liner. It is in essence an extension of the Cargill code. In their paper, the analytical model is verified against the FE method of ACTRAN, and results of both methods are found to be comparable. The verification is, however, done for a specific case limited to a single combination of frequenty and liner impedance, and more research on the subject is proposed. In chapter six of his 2013 thesis for the degree of Doctor of Philosophy, Mustafi [9] uses the analytical Cargill code to predict the behaviour of noise scattering due to a acoustically hard patch in the lining as a result of damage and repair of the lining. Results are again tested against the full 3D FE method of ACTRAN. Good agreement was found when modelling relatively small patches (width $< 1\%$ of the duct circumference). Poor agreement is found when modelling wider patches.

Finally, in their 2008 paper, Gabard and Astley [10] propose a mode-matching FE method to solve the problem of sound scattering in a duct, the duct in this case being composed of several axial segments of finite length, each segment having the same cross-section but circumferentially varying impedance. The goal of the method is to find the conditions to match the solutions on either side of an interface between two of these sections. The matching is based upon the time harmonic linearized momentum and continuity equations for incviscid, parallel flow. The matching conditions are then used to match modal solutions across a liner discontinuity. Again, ACTRAN is used to validate the model. It is concluded that the model provides a practical tool for predicting far-field radiation patterns for 3D lined bypass ducts at frequencies and flow conditions of practical interest.

Objective and problem definition

The objective of this report is to test the feasability of a iterative method for numerically solving the sound transmission in a lined duct with hard patches and splices. The main two problems with existing methods for computing the sound propagation through a duct, are computational costs and model limitations. As said before, a full three dimensional Finite Element Analysis may be very universal in its use for ducts of different shapes in different conditions, it is also very computationally expensive. A (semi-)analytical code as the Cargill code, on the other hand, is computationally cheap but limited in its duct geometry. The method tested in this report is based on the Cargill code, extended with an iterative process in order to account for the non-axisymmetric lining as a result of the inclusion of liner splices and patches.

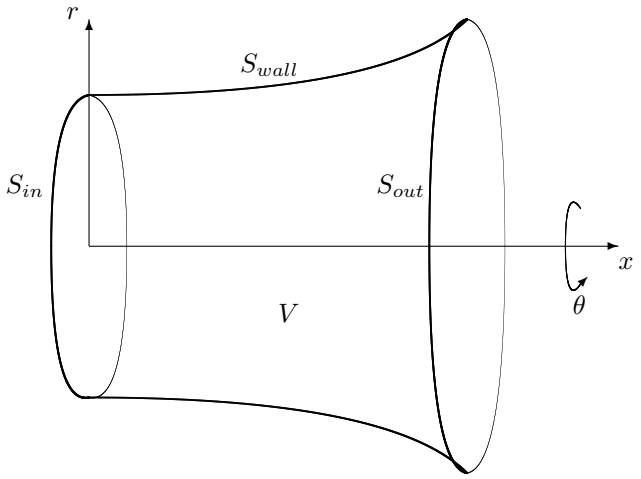

Figure 1: Numbering of nodes (italic) and elements (bold) in a 2D mesh with $N_x = 4$ and $N_r = 3$.

To test the feasability of the method, a Matlab code will be developed to handle the simplified case of a circular duct, axi-symmetric in its geometry, in absence of mean flow. Figure 1 shows the geometry of such a duct, where V is the total volume of the duct and S_{in}, S_{out} and S_{wall} are the inlet, outlet and wall surfaces, respectively. The Matlab code is based on a Finite Element approximation similar to the Cargill code, discretizing the problem on a computational grid and solving for reflecting and transmitted wave modes at the inlet and outlet of the duct as a result of a specific incident mode. The difficulties of the inclusion of lining discontinuities such as splices and patches into the model arise due to the fact of the mode scattering. As will be shown in this report, the scattering of the modes results in a coupled set of equations, which may be solved using the iterative method.

The problem of sound propagation in a non-axisymmetric lined duct is divided in three different sub-problems;

- The 1D eigenproblem for radial modes at inlet and outlet of the duct,
- The 2D transmission problem for axisymmetric lined ducts for a specific incident azimuthal mode m,
- The 2D transmission problem for non-axisymmetric lined ducts, coupeling the equations for incident azimuthal mode m and scattered azimuthal modes n.

Each of these sub-problems will be discussed in more detail in later sections. The first part of the report discusses the mathematics of each sub-problem. The second part of this report discusses the developed Matlab code to solve each sub-problem separately and consequently the entire problem as a whole. In the last part of this report the results of each sub-problem will be presented, followed by some conclusions on the feasability of the method and notes on future work.

3 1D Eigenproblem

Figure 2 shows the two dimensional duct geometry for a specific $\theta = constant$ for a circular duct with constant radius R. An axisymmetric hard-walled area exists at the inlet area for $0 \leq x \leq x_1$ and at the outlet area for $x_2 \leq x \leq L$. Along the wall (boundary Γ_{wall}), acoustic lining with a specific admittance A is placed for $x_1 \leq x \leq x_2$.

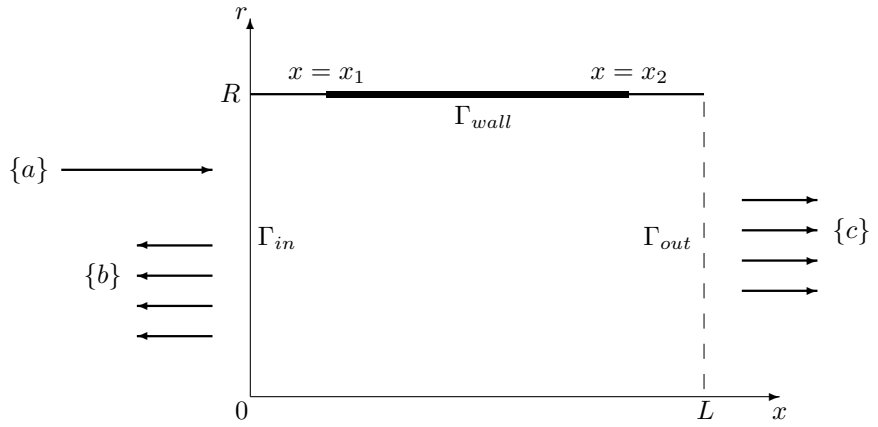

Figure 2: Schematic view of the 2D representation of a duct with length L and radius R with hard-walled inlet section along boundary Γ_{wall} for $0 \leq x \leq x_1$ and $x_2 \leq x \leq L$. The section of Γ_{wall} between x_1 and x_2 is either hard-walled ($A = 0$) or lined ($A \neq 0$). An incident wave of modal amplitudes $\{a\}$ results in reflected and transmitted waves of modal amplitudes $\{b\}$ and $\{c\}$, respectively.

The incident, reflected and transmitted sound waves are represented in figure 2 by their amplitude vectors $\{a\}$, $\{b\}$ and $\{c\}$, respectively, so that the inlet pressure distribution p_{in} along boundary Γ_{in} and the outlet pressure distribution p_{out} along boundary Γ_{out} may be written as the infinite sums

$$\begin{aligned} p_{in} &= \sum_{n=1}^{\infty} a_n f_n^+ + \sum_{n=1}^{\infty} b_n f_n^-, \\ p_{out} &= \sum_{n=1}^{\infty} c_n g_n^+, \end{aligned} \tag{1}$$

where f_n^+ and g_n^+ denote eigenfunctions traveling in the positive x-direction and f_n^- denote eigenfunctions traveling in the negative x-direction. By matching these pressure distributions on the one dimensional inlet and outlet boundaries to the two dimensional transmission problem, the two dimensional transmission problem can be fully defined. This section describes the analytical formulation, the solution and the numerical solver of the one dimensional eigenproblem for the pressure distributions along the inlet and outlet areas of the duct.

Analytical formulation

Since for the feasability study described in this report the simplified problem of no flow is considered, the governing equation for sound propagation is the Helmholtz equation,

$$\nabla^2 p + k^2 p = 0, \tag{2}$$

for any wave number k. When considering a lined, geometrically axi-symmetric duct, the boundary conditions enclosing the problem are found in the specific wall admittance A,

$$\begin{aligned} \left.\frac{\partial p}{\partial r}\right|_{r=r_1} &= \imath k A_1 p, \\ \left.\frac{\partial p}{\partial r}\right|_{r=r_2} &= -\imath k A_2 p, \end{aligned} \tag{3}$$

which describe the effect of the lower duct boundary (subscript 1) and the upper duct boundary (subscript 2) on the acoustic field. In this report, unless stated otherwise, the lower boundary will correspond with the centreline of the duct ($A_1 = 0$) and the upper boundary will correspond with the duct wall, which is either acoustically hard ($A_2 = 0$) or lined ($A_2 \neq 0$). A solution to the Helmholtz equation can be found using the method of separation of variables,

$$p^* = p(r) e^{\imath m \theta} e^{-\imath k \lambda x}, \tag{4}$$

which allows the solution field p^* to be written as a function of radial component r for an infinite number of azimuthal modes m and axial wave numbers $k\lambda$. Substitution of this solution into equation 2 gives

$$\frac{1}{r}\frac{\partial}{\partial r}\left(r\frac{\partial p}{\partial r}\right) + \left\{k^2(1-\lambda^2) - \frac{m^2}{r^2}\right\} p = 0, \tag{5}$$

which may also be written in form of a weak formulation as

$$\int_{r_1}^{r_2} W(r) \left\{\frac{1}{r}\frac{\partial}{\partial r}\left(r\frac{\partial p}{\partial r}\right) + \left(k^2(1-\lambda^2) - \frac{m^2}{r^2}\right) p\right\} r\, dr = 0 \tag{6}$$

for all $W(r)$. After integrating the first term by parts, one obtains the expression

$$\int_{r_1}^{r_2} -\frac{dW}{dr}\frac{dp}{dr} r\, dr + \int_{r_1}^{r_2} k^2(1-\lambda^2) W p r\, dr - m^2 \int_{r_1}^{r^2} W p \frac{1}{r} dr + \left[W r \frac{dp}{dr}\right]_{r_1}^{r_2} = 0, \tag{7}$$

where the last term on the left hand side of the equation can be replaced by the boundary conditions (3) so that

$$\left[W r \frac{dp}{dr}\right]_{r_1}^{r_2} = -\imath k A_2 r_2 p(r_2) W(r_2) - \imath k A_1 r_1 p(r_1) W(r_1). \tag{8}$$

FE formulation

In order to solve equation 7 at the inlet $x = 0$ and outlet $x = L$ of the duct, the problem is discribed using a finite element formulation on a one dimensional computational grid in radial

direction,

$$p(r) = \sum_{i=1}^{N_r+1} N_i(r) p_i, \tag{9}$$

where N_r is the number of finite elements in radial direction and N_i is the shape function in node i. Substituting equations 8 and 9 into equation 7 and choosing weight functions W_i equal to the shape functions N_i gives the governing set of equations,

$$\left\{[A] + k^2(1-\lambda^2)[B] - m^2[C] - \imath k A_2[D_2] - \imath k A_1[D1]\right\}\{p\} = 0, \tag{10}$$

where matrices $[A]$, $[B]$, $[C]$, $[D_1]$ and $[D_2]$ are assembled out of the components of the elemental matrices $[A]^2$, $[B]^e$, $[C]^e$, $[D_1]^e$ and $[D_2]^e$, which are given by

$$\begin{aligned}
[A]^e &= \int_a^b -[N]_r^{e^T}[N]_r^e r\, dr, \\
[B]^e &= \int_a^b [N]^{e^T}[N]^e r\, dr, \\
[C]^e &= \int_a^b [N]^{e^T}[N]^e \frac{1}{r}\, dr, \\
[D_\alpha]^e &= \left[r[N(r)]^{e^T}[N(r)]^e\right]_{r=r_\alpha}, \ \alpha = 1, 2.
\end{aligned} \tag{11}$$

The set of equations 10 can be rewritten to form an eigenproblem

$$\left\{[E_1] - \lambda^2 k^2 [E_2]\right\}\{p\} = 0, \tag{12}$$

where

$$\begin{aligned}
[E_1] &= [A] + k^2[B] - m^2[C] - \imath k A_2[D_2] - \imath k A_1[D1], \\
[E_2] &= [B].
\end{aligned} \tag{13}$$

The eigenproblem of equation 12 can now be solved at one dimensional grids with a number of elements N_r at the inlet and outlet of the duct for a specific azimuthal mode number m by choosing appropriate shape functions N_i, resulting in a number N_r of eigensolutions. In this report, the computational grid is built up from simple, linear elements. For the one dimensional grids in radial directions this means, with the nodes of the element at $r = a$ and $r = b$,

$$p(r) = N_a(r) p_a + N_b(r) p_b, \tag{14}$$

with

$$\begin{aligned}
N_a(r) &= \frac{b-r}{b-a}, \\
N_b(r) &= \frac{r-a}{b-a}.
\end{aligned} \tag{15}$$

Each eigensolution p_n with eigenvalue $k\lambda_n$ now corresponds to a radial mode $n = \mu$ for $\mu \in [1, N_r]$,

so that, for example for the first eigensolution of equation 12 at the outlet area of the duct,

$$g_\mu^+ = \{p\}_\mu e^{-\imath k \lambda_\mu x}, \tag{16}$$

where $\{p\}_\mu$ and $k\lambda_\mu$ form the μth eigensolution to equation 12 solved at the outlet grid.

Normalization

Each resulting radial mode shape $\{p\}_\mu$ that comes with a specific eigenvalue λ_μ for a specific azimuthal mode m is normalized such that the average intensity of the one dimensional pressure field over the duct cross-section is equal to one;

$$\begin{aligned} \bar{I}_m &= \frac{Re(\lambda_m)}{2\rho_0 c_0} \frac{\int_{r_1}^{r^2} 2\pi |p_m(r)|^2 r\, dr}{\pi(r_2^2 - r_1^2)} = \alpha^2, \\ \{p_m\}_{av} &= \frac{1}{\alpha}\{p_m\}. \end{aligned} \tag{17}$$

Substituting the discretized values for $p_m(r)$ enables the integral term in equation 17 to be calculated using the matrix $[B]$ from equations 11,

$$\int_{r_1}^{r^2} |p_m(r)|^2 r\, dr = \int_{r_1}^{r^2} [N]^T \{p_m\}^T [N] \{p_m^*\} r\, dr = \{p_m\}^T [B] \{p_m^*\}. \tag{18}$$

Furthermore, the direction of the eigenvector is normalized such that the pressure field is real and positive on the duct wall;

$$\{p_m\}_{norm} = \frac{|p_{m_{av}}|_{wall}}{(p_{m_{av}})_{wall}} \{p_m\}_{av}. \tag{19}$$

Finally, the resulting eigenvalues and subsequently the accompanying eigenvectors are sorted based on the degree to which they are 'cut on': all eigenvalues are sorted in ascending order based on their imaginary part, where, if present, the first few fully cut on modes with an imaginary part equal to zero are sorted in descending order. In the remainder of this report, the subscript *norm* will not be taken and each mention of the pressure field $\{p_m\}$ will refer to the *normalized* pressure field.

4 2D Transmission in axisymmetric lined ducts

Similar to the way discussed in the previous section for the one dimensional problem, a finite element formulation can be found for the problem of sound transmission through a two dimensional duct with axisymmetric lining. The one dimensional solutions of previous section are subsequently used to define the incident, transmitted and reflected wave modes at the boundaries of the two dimensional duct. The finite element formulation is equal to the one proposed by Astley and Eversman in 1978 [3] and is briefly illustrated in this section.

Analytical formulation

The formulation of the analytical problem of the pressure field inside the two dimensional duct is based upon the same equations as the one dimensional problem described in previous section, meaning the Helmholtz equation (equation 2) and the boundary conditions of equation 3. The difference with the one dimensional analysis is the substituted variable-separated solution, which is now two dimensional so that, for a circular duct,

$$p^* = p(x,r)e^{\imath m\theta}e^{-\imath k\lambda x}. \tag{20}$$

Substituting this solution into the Helmholtz equation again allows the problem to be written in the form of a variational statement including the constant admittance boundary conditions at the upper and lower boundary of the duct,

$$\int_R \left(\nabla W_i \nabla p - \left(k^2 - \frac{m^2}{r^2}\right) pW_i\right) dR + \int_{\Gamma_{wall}} \imath kApW_i \, dS + \int_{\Gamma_{in}} W_i p_{in_x} \, dS - \int_{\Gamma_{out}} W_i p_{out_x} \, dS \tag{21}$$

Where R is the duct area, Γ_{wall} is the duct wall boundary, Γ_{in} is the duct inlet boundary and Γ_{out} is the duct outlet boundary. The problem is further defined by stating boundary conditions for the inlet and outlet boundary, matching the modal solutions of the 1D eigenproblem of previous section to these boundaries of the 2D duct. These boundary conditions state that the pressure field does not change over the inlet and outlet cross-sections. In variational form using weight functions F_j and G_k this can be written as

$$\begin{aligned} \int_{S_{in}} (p_{in} - p)F_j \, dr = 0, \\ \int_{S_{out}} (p_{out} - p)G_k \, dr = 0. \end{aligned} \tag{22}$$

FE formulation

The finite element formulation of the analytical problem stated above is again the result of discretizing the solution field $p(x,r)$ on to a computational grid, using appropriate shape functions N_i. A complete set of finite element equations for the two dimensional sound transmission appears by setting the weight functions W_i in the variational statement 21 equal to the weight functions N_i, and setting weight functions F_j and G_k in equations 22 equal to the derivatives of the 1D solution fields $f^-_{\mu_x}$ and $g^+_{\mu_x}$, respectively. The resulting set of equations can be written in matrix form as

$$\begin{bmatrix} [K_b] & [B]^T & 0 \\ [B] & [K] & [C] \\ 0 & [C]^T & [K_c] \end{bmatrix} \begin{Bmatrix} \{b\} \\ \{p\} \\ \{c\} \end{Bmatrix} = \begin{bmatrix} -[K_{ba}] \\ -[A] \\ 0 \end{bmatrix} \{a\}, \tag{23}$$

where

$$\begin{aligned}
[K]^e &= [K_1]^e + [K_2]^e \\
[K_1]^e &= 2\pi \int_{R_e} \left([N]_x^{e^T} [N]_x^e + [N]_r^{e^T} [N]_r^e - \left(k^2 - \frac{m^2}{r^2} \right) [N]^{e^T} [N]^e \right) r \, dr \, dx, \\
[K_2]^e &= 2\pi \int_{C_3^e} \imath k A [N]^{e^T} [N]^e r \, dS, \\
[A]^e &= 2\pi \int_{C_1^e} [N]^{e^T} [f^+]_x r \, dr, \\
[B]^e &= 2\pi \int_{C_1^e} [N]^{e^T} [f^-]_x r \, dr, \\
[C]^e &= 2\pi \int_{C_2^e} -[N]^{e^T} [g^+]_x r \, dr, \\
[K_b] &= 2\pi \int_{C_1} -[F]^T [f^-] r \, dr, \\
[K_{ba}] &= 2\pi \int_{C_1} -[F]^T [f^+] r \, dr, \\
[K_c] &= 2\pi \int_{C_2} [G]^T [g^+] r \, dr.
\end{aligned} \tag{24}$$

In equations 24, the superscript e in $[X]^e$ means $[X]^e$ is an elemental part of global matrix $[X]$ so that $[X] = \sum_e [X]^e$. Substituting the appropriate weight functions and incident, reflected and transmitted modes gives

$$\begin{aligned}
[A]^e &= 2\pi \int_{C_1^e} [N]^{e^T} (-\imath [N][p_1] e^{-\imath [D_1] x_1} [D_1]) r \, dr, \\
[B]^e &= 2\pi \int_{C_1^e} [N]^{e^T} (\imath [N][p_1] e^{\imath [D_1] x_1} [D_1]) r \, dr, \\
[C]^e &= 2\pi \int_{C_2^e} -[N]^{e^T} (-\imath [N][p_2] e^{-\imath [D_2] x_2} [D_2]) r \, dr, \\
[K_b] &= 2\pi \int_{C_1} -\left(\imath [N][p_1] e^{\imath [D_1] x_1} [D_1] \right)^T \left([N][p_1] e^{\imath [D_1] x_1} \right) r \, dr, \\
[K_{ba}] &= 2 \int_{C_1} -\left(\imath [N][p_1][D_1] \right)^T \left([N][p_1] \right) r \, dr, \\
[K_c] &= 2\pi \int_{C_2} \left(-\imath [N][p_2] e^{-\imath [D_2] x_2} [D_2] \right)^T \left([N][p_2] e^{-\imath [D_2] x_2} \right) r \, dr,
\end{aligned} \tag{25}$$

for a specific circumferential mode number m. In these equations, $[p_\alpha]$ is the radial mode shape matrix whose columns the eigenvectors that form part of the solution to the one dimensional eigenproblem described in previous chapter and matrix $[D_\alpha]$ is the diagonal matrix whose diagonal elements contain the corresponding eigenvalues, with $\alpha = 1$ for the duct inlet and $\alpha = 2$

for the duct outlet solutions. By choosing $x_2 = 0$ rather than $x_2 = L$ in equations 25, the transmitted modal amplitudes $\{c\}$ are relative to the outlet area rather than the inlet area.

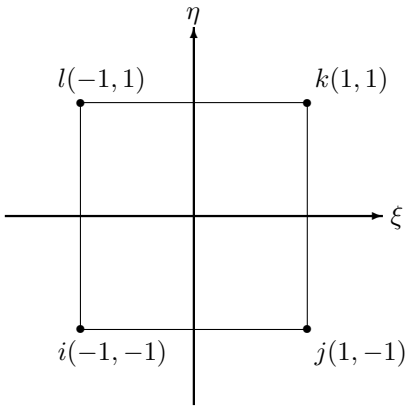

Figure 3: Shape of arbitrary element in local coordinates.

In this report, the set of equations 23 is solved on a mesh consisting of linear, rectangular elements. The elements used are *isoparametric* elements, meaning that for each element positioned in the global x, r-coordinate system, the shape functions can be defined in terms of local coordinates ξ and η. They are are defined such that, in this local coordinate system, the boundaries of the element correspond to the constant values $\xi = -1$, $\xi = 1$, $\eta = -1$ and $\eta = 1$ as seen in figure 3. The shape functions defining the shape of the element in the global x, r-coordinate system in terms of local coordinates ξ and η are

$$\begin{aligned} N_i &= \frac{1}{4}(1-\xi)(1-\eta), \\ N_j &= \frac{1}{4}(1+\xi)(1-\eta), \\ N_k &= \frac{1}{4}(1+\xi)(1+\eta), \\ N_l &= \frac{1}{4}(1-\xi)(1+\eta). \end{aligned} \tag{26}$$

Furthermore, writing the elemental stiffness matrices of equations 24 as a function of the local coordinates ξ and η involves the following transformations

$$\begin{aligned} \left\{ \begin{array}{c} x \\ r \end{array} \right\} &= \left\{ \begin{array}{c} \sum N_i x_i \\ \sum N_i r_i \end{array} \right\}, \\ \left\{ \begin{array}{c} [N]_x \\ [N]_r \end{array} \right\} &= [J]^{-1} \left\{ \begin{array}{c} [N]_\xi \\ [N]_\eta \end{array} \right\}, \\ \int (...)\, dr\, dx &= \int (...)|J|\, d\xi\, d\eta, \end{aligned} \tag{27}$$

where $[J]$ is the Jacobian given by

$$[J] = \left[\begin{array}{cc} x_\xi & y_\xi \\ x_\eta & y_\eta \end{array} \right]. \tag{28}$$

5 2D Transmission in non-axisymmetric lined ducts

Non-axisymmetric lining in the axi-symmetric (circular) duct considered so far, is mathematically described by a wall admittance $A(x, \theta)$ varying with azimuthal angle θ. This section described the approach of writing admittance $A(x, \theta)$ in terms of a complex Fourier expansion and the steps necessary to implement this in the governing equations deduced so far.

Admittance as complex Fourier expansion

Non-axisymmetric lining $A(x, \theta)$ of an axi-symmetric duct can be written as a complex Fourier expansion in θ;

$$A(x, \theta) = \sum_{n=-\infty}^{\infty} A^n(x) e^{\imath n \theta}, \tag{29}$$

with

$$A^n(x) = \frac{1}{2\pi} \int_{-\pi}^{\pi} A(x, \theta) e^{-\imath n \theta} \, d\theta. \tag{30}$$

It is assumed that along the circular boundary of the duct, at a specific position x, admittance $A(x, \theta) = A$ everywhere (i.e. for $\pi \leq \theta \leq \pi$) except for a small hard-walled area $\epsilon/2 \leq \theta \leq \epsilon/2$, with $\epsilon \leq 2\pi$, where $A(x, \theta) = 0$ (representing for example a liner splice or patch). Evaluating the integral in equation 30 for this specific assumed admittance gives

$$\begin{aligned} A^n(x) = A^{-n}(x) &= -\frac{\epsilon A}{\pi} \left(\frac{\sin \frac{n\epsilon}{2}}{n\epsilon} \right) \text{ for } n \neq 0, \\ A^0(x) &= A \left(1 - \frac{\epsilon}{2\pi} \right) \text{ for } n = 0. \end{aligned} \tag{31}$$

Figure 4 shows plots of equations 31 substituted into equation 29 with $A = 1$ and $\epsilon = \frac{1}{16}\pi$, for $n \in [-10, 10]$, $n \in [-100, 100]$ and $n \in [-1000, 1000]$.

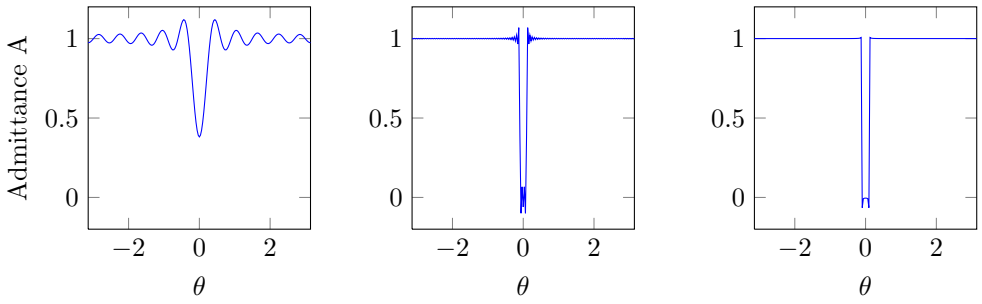

Figure 4: Plots of the admittance written as a Fourier expansion for $n \in [-10, 10]$ (left), $n \in [-100, 100]$ (middle) and $n \in [-1000, 1000]$ (right).

Implementation in governing equations

The governing system of equations for implementing the non-axisymmetric admittance $A(x, \theta)$ is, written in the notation of equation 23:

$$[B^m]\{b^m\} + [K^m]\{p^m\} + [C^m]\{c^m\} = -[A^m]\{a^m\} \tag{32}$$

for a specific incident azimuthal mode m. In equation 32, $[K^m] = [K_1^m] + [K_2]$ and the term dependent on the admittance is

$$[K_2]\{p^m\} = \left[2\pi \int_{C_3} \imath k A [N]^T [N] r \, dS\right] \{p^m\}. \tag{33}$$

Substituting equations 31 and 29 into equation 32 gives

$$[B^m]\{b^m\} + \left[[K_1^m] + [K_2]^0\right] \{p^m\} + [C^m]\{c^m\} = -[A^m]\{a^m\} - \{f^m\}, \tag{34}$$

where

$$\{f^m\}^e = 2\pi \sum_{q \neq 0} \left[\int_{C_3^e} \imath k A^q [N]^{e^T} [N]^e \, dS\right] \{p^{m-q}\} = \sum_{q \neq 0} \frac{A^q}{A^0} [K_2]^{0^e} \{p^{m-q}\} \tag{35}$$

for $q \in [-\infty, \infty]$, $[K_2]^0 = [K_2]$ evaluated for $A = A^0$ and azimuthal mode number $n = m$. For all other azimuthal mode numbers $n \neq m$, the incident mode term disappears from the equations, resulting in

$$[B^n]\{b^n\} + \left[[K_1^n] + [K_2]^0\right] \{p^n\} + [C^n]\{c^n\} = -\{f^n\}, \tag{36}$$

Iterative solver

Equations 34, 35 and 36 show that, for an non-axisymmetric lining written as a complex Fourier series, each solution $\{p^m\}$ for incident azimuthal mode m is dependent on all modal solutions $\{p^{m-q}\}$ for $q \in [-\infty, \infty]$. The system is solved iteratively following the following steps:

1. Truncate the infinite series in equation 35 after a fixed number of M terms on either side, so that $q \in [-M, M]$ and $n \in [m-M, m-M+1, ..., m-1, m, m+1, ..., m+M]$, resulting in a total number of $2M+1$ equations.
2. Set all initial solutions $\{p^n\}$ equal to zero.
3. Solve equation 34 for $\{p^m\}$. For the first iteration, due to the initial values defined in step 2, $\{f^m\} = 0$. The outcome is an *estimation* $\{\tilde{p}^m\}$.
4. Solve equation 36 for all $\{p^n\}$, $n \neq m$. Again, $\{f^n\} = 0$ at the start of the first iteration. During a single iteration, depending on Gauss-Seidel or Jacobi iterations, preliminary estimations $\{\tilde{p}^n\}$ for all $n < N$ may or may not be substituted in equation 36 when solving for $\{\tilde{p}^N\}$. The outcome are estimations $\{\tilde{p}^n\}$ for all $n \neq m$.
5. Substitute new estimations $\{\tilde{p}^n\}$ into equation 34 and again solve this equation for $\{p^m\}$, resulting in a new estimation $\{\tilde{p}^m\}$.
6. Substitute new estimations $\{\tilde{p}^n\}$ into equation 36 and again solve this equation for all $\{p^n\}$, $n \neq m$, resulting in new estimations $\{\tilde{p}^n\}$.
7. Repeat steps 5 and 6 until limit of convergence for $\{\tilde{p}^m\}$ is reached.

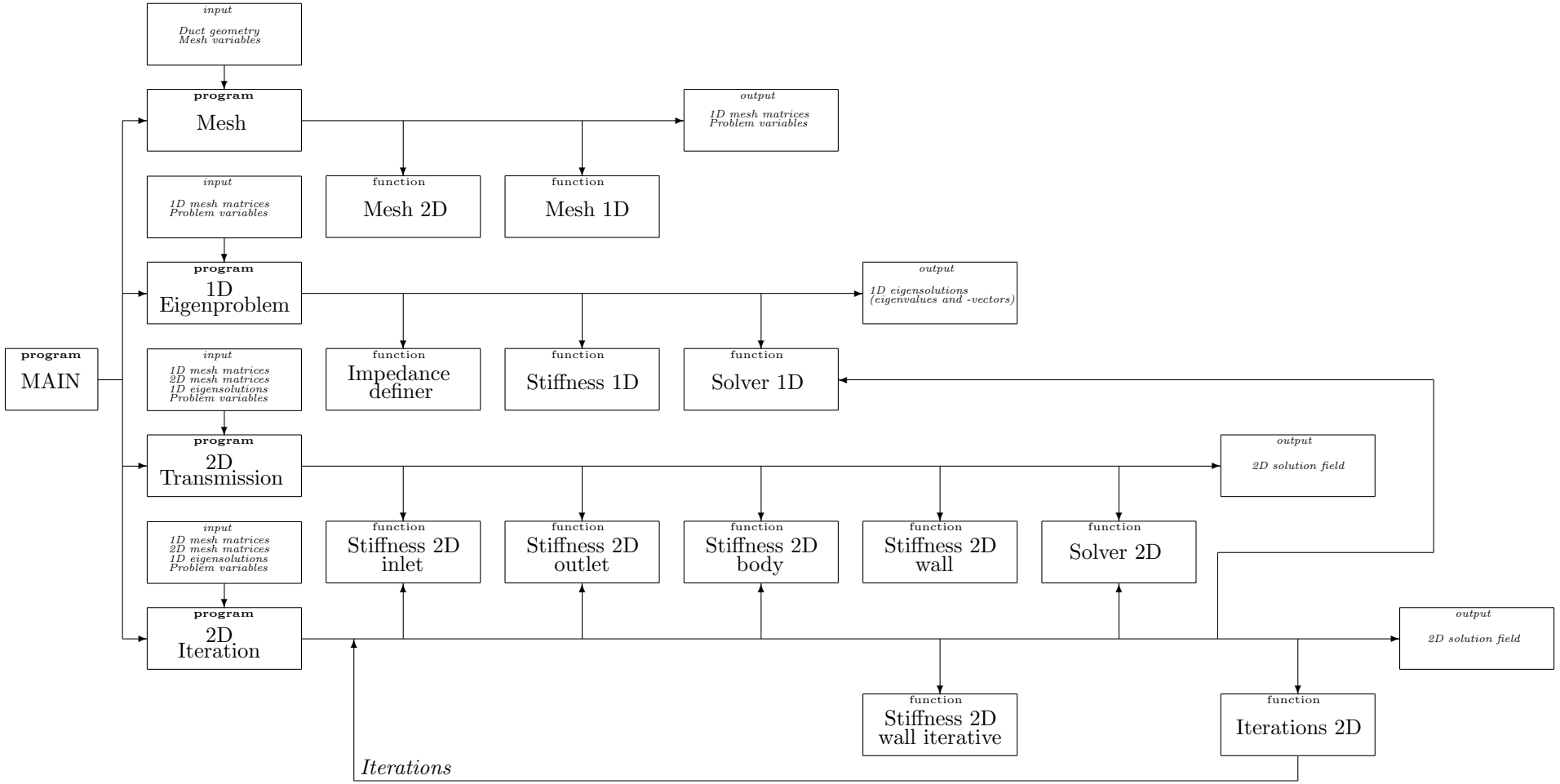

Figure 5: Program structure of the complete Matlab solver.

6 Matlab program layout

Figure 5 shows the complete lay-out of program and functions files of the MatLab code that has been written in order to solve the problems described in previous chapters. Four seperate sub-programs have been written for the four main functions of the code:

- Creating a computational mesh of finite elements (program file: *Mesh*)
- Solving the 1D eigenproblem for the incident modes (program file: *1D Eigenproblem*)
- Solving the 2D transmission problem for the incident modes in case of axisymmetric lining (program file: *2D Transmission*)
- Solving the 2D transmission problem iteratively for non-axisymmetric lining (program file: *2D Iteration*)

Each of this four sub-programs can be used as a stand-alone program, provided the necessary data-files are present. For each sub-program, several function files are written to assist the main goal of each sub-program. The main program (program file: *MAIN*) calls to the four different sub-programs based on what the user desires the code to compute. In this chapter, the working of each of the four sub-programs will be illustrated.

Mesh

The sub-program *Mesh*, using function files *Mesh 2D* and *Mesh 1D*, is responsible for creating a two dimensional computational mesh of a duct of specific geometry and four one dimensional computational meshes along the four boundaries of the duct (being the inlet, outlet, bottom and top boundary). Based on user input on duct geometry and mesh specifications, the function file *Mesh 2D* creates a structured two dimensional mesh of the duct consisting of simple, rectangular elements. Restrictions are that the duct is either circular or annular. Its top and bottom boundary descriptions can either be a real number a, corresponding to a straight boundary parallel to the x-direction at $r = a$, or a continuous function $a(x)$ corresponding to a boundary shape varying with x. The result is a structured mesh with nodes and elements numbered according to figure 6.

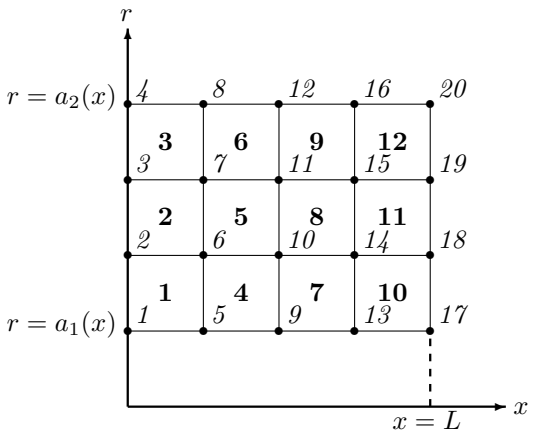

Figure 6: Numbering of nodes (italic) and elements (bold) in a 2D mesh with $N_x = 4$ and $N_r = 3$.

The output of the function *Mesh 2D* consists of a matrix ELM_2D, size $N_{2D} \times 5$, and a matrix NOD_2D, size $n_{2D} \times 3$, where N_{2D} is the total number of elements and n_{2D} is the total number of nodes in the 2D mesh (see figure 7). The matrix ELM_2D contains in the first column the element number, in the second column the number of the lower left node (nll), in the third column the number of the lower right node (nlr), in the fourth column the number of the upper right node (nur) and in the fifth column the number of the upper left node (nul) of each element. The matrix NOD_2D contains in the first column the node number, in the second column the x-position and in the third column the r-position of each node.

Element number	nll	nlr	nur	nul
1	1	5	6	2
2	2	6	7	3
3	3	7	8	4
⋮	⋮	⋮	⋮	⋮
12	15	19	20	16

Node number	x	r
1	0.0	$a_1(0)$
2	0.0	r_2
3	0.0	r_3
⋮	⋮	⋮
20	L	$a_2(L)$

Figure 7: 2D Mesh output matrices ELM2D (left) and NOD2D (right) for a mesh with $N_x = 4$ and $N_r = 3$.

The second function of the sub-program *Mesh* is to create one dimensional meshes at specific cross-sections, with nodes corresponding to the two dimensional mesh. Additional output to the function *Mesh_2D* is a one dimensional mesh along the boundary $r = a_2(x)$, such that the nodes of this mesh coincide with the upper wall nodes of the two dimensional mesh. The function *Mesh_1D* creates one dimensional meshes for specific cross-sections of the duct at some specific constant $x = b$, given as input by the user. Further input to this function are existing two dimensional mesh matrices with a structure similar to the output matrices of the function *Mesh_2D*.

The output files of all one dimensional meshes consist of a matrix ELM_1D, size $N_{1D} \times 3$, and a matrix NOD_1D, size $n_{1D} \times 3$, where N_{1D} is the number of elements and n_{1D} is the number of nodes in the 1D mesh (see figure 8 for an example at the duct inlet). The matrix ELM_1D contains in the first column the element number, in the second column the number of the lower node (nl) and in the third column the number of the upper node (nu) of each element. The matrix NOD_1D contains in the first column the node number, in the second column the x-position and in the third column the r-position of each node. Elements and nodes are numbered from 1 to N_{1D} and from 1 to n_{1D} respectively, where element and node number 1 correspond to the element or node at $r = a_1(b)$ and element and node number N_{1D} and n_{1D} correspond to respectively the element and node at $r = a_2(b)$.

Element number	nl	nu
1	1	2
2	2	3
3	3	4

Node number	x	r
1	0.0	$a_1(0)$
2	0.0	r_2
3	0.0	r_3
4	0.0	$a_2(x)$

Figure 8: 1D Mesh output matrices ELM1D (left) and NOD1D (right) for the duct input cross-section at $x = 0$ of a mesh with $N_x = 4$ and $N_r = 3$.

The 1D mesh along the upper wall $r = a_2(x)$ which is given as additional output to the function *Mesh_2D* is represented by elemental and nodal matrices *ELM_1D_wall* and *NOD_1D_wall* with structures similar to the 1D nodal and elemental matrices depicted in figure 8, with the only difference that the matrix *NOD_1D_wall* contains an extra fourth column in which the wall impedance at each wall node can be stored.

1D Eigenproblem

The sub-program *1D Eigenproblem* consists of functions *Impedance definer*, *Stiffness 1D* and *Solver 1D*. The function *Impedance definer* lets the user define the admittance at the upper wall of the duct, filling the fourth column of the nodal matrix *NOD_1D_wall*. It also lets the user define a patch, giving as output a vector *ELM_1D_patch* which contains the number of the elements that are associated with the patch.

The function *Stiffness 1D* generates the stiffness matrices of the one dimensional eigenvalue problem for any one dimensional grid. Input to the function are any matrices NOD_1D and ELM_1D. The function loops over the number of elements numbered in matrix ELM_1D and obtaines from it the numbers of the lower and upper node of each element. From the matrix NOD_1D it obtaines subsequently the x- and r-position of these nodes. Based on this information, it generates for each element the elemental stiffness matrices $[A]^e$, $[B]^e$ and $[C]^e$ according to equations 11 and 15. For the two boundary elements it also generates stiffness matrices $[D_1]^e$ and $[D_2]^e$. Numerical integration is done using a two point Gauss Quadrature.

Each component of the elemental stiffness matrices is summed to its corresponding position in the global stiffness matrices $[A]$, $[B]$, $[C]$, $[D_1]$ and $[D_2]$, which initialy contain zeros only. Global stiffness matrix elements A_{ij} $(i = 1, 2, ..., n_{1D};\ j = 1, 2, ..., n_{1D})$ correspond to the i^{th} and j^{th} node stored in the matrix NOD_1D. The same is true for global stiffness matrix elements B_{ij}, C_{ij} and D_{ij}. If, for example, a perticular element X consists of lower node f and upper node g, and node f and node g have respectively positions i and j in the matrix NOD_1D, then A^e_{ff} corresponds to A_{ii}, A_{fg} corresponds to A_{ij}, etc.

The function *Solver 1D* solves the one dimensional eigenproblem (equation 12) which is set up by the input of stiffness matrices $[A]$, $[B]$, $[C]$, $[D_1]$ and $[D_2]$ and additional input consisting of the angular wave frequency k, the circumferential mode number m and the boundary impedance values A_1 and A_2 at the specific value x of the 1D mesh. The solving of the problem is done using Matlab's eigenvalue solver *eig*. Furthermore, the function normalizes the result according to equations 17 and 19. The output of the function consists of a diagonal matrix $[D]$ of eigenvalues $k^2\lambda^2$, a full matrix $[V]$ whose columns are the corresponding eigenvectors and a vector $\{k\lambda\}$ containing all found roots of the eigenvalues corresponding to the axial wave numbers of equation 4. For bigger meshes, the user can choose to store a specific number of eigensolutions, rather than the total number of resulting eigensolutions which is equal to the number of nodes in the one dimensional mesh.

2D Transmission

The sub-program *2D Transmission* consists of the functions *Stiffness 2D inlet*, *Stiffness 2D outlet*, *Stiffness 2D body*, *Stiffness 2D wall* and *Solver 2D*. The first four of these functions evaluate the stiffness matrices in equation 24 using a loop over each finite element in the two dimensional grid, numerically solving the integral using a two point Gauss quadrature and summing the ele-

ments of the resulting elemental matrices to the correct position in the global stiffness matrices, similar to the way described in the section on the sub-program *1D Eigenproblem*. The function *Solver 2D* solves the system of equations 23 by assembling all two dimensional stiffness matrices together to form a single set of equations,

$$[M]\{P\} = \{V\}, \tag{37}$$

where $[M]$ equals the total left hand matrix of system of equations 23, $\{V\}$ the total right hand side of the system and $\{P\}$ the total solution vector consisting of $\{b\}$, $\{p\}$ and $\{c\}$.

The number of 1D eigensolutions used in evaluating the boundary matrices $[K_b]$, $[K_{ba}]$ and $[K_c]$ can be defined by the user. When the user chooses to use all available eigensolutions, the number of solutions used for the evaluation is limited to 20, for bigger numbers may lead to matrix $[M]$ being singular, resulting in the problem not being able to be solved. Further user input consists of the vector $\{a\}$, defining the incident mode amplitudes. The output consists of the two dimensional solution field $\{p\}$ and the reflected and transmitted mode amplitude vectors $\{b\}$ and $\{c\}$.

For circular ducts and azimuthal modes $m \neq 0$, all elements in all rows and columns in matrix $[M]$ associated with the solutions p_n for nodes located at the centre of the duct are replaced by zero, except for the elements located at the diagonal of the matrix $[M]$ which are replaced by the average value of the diagonal. This way the numerical solution is forced to equal zero at the centre of the duct, which resembles the exact solution as will be shown in the results section.

2D Iteration

The sub-program *2D Iteration* solves the full set of equations described in section 5 using the iterative procedure. It uses all *Stiffness* functions from the sub-program *2D Transmission*, replacing the function *Stiffness 2D wall* by the function *Stiffness 2D wall iterative* to account for the change in admittance from a constant value A to a fourier series $A(x, \theta)$. Furthermore, it uses the *Solver 1D* function from the sub-program *1D Eigenproblem* to solve the incident, reflected and transmitted radial modes for each non-incident azimuthal mode n and it uses the function *Iterations 2D* to iterate the process.

The input to the sub-program *2D Iteration* is equal to the input to the sub-program *2D Transmission*, extended by the value ϵ defining the circumferential width of the patch and the value M truncating the infinite Fourier series for the admittance and subsequently defining the number of non-incident modes $n \in [m - M, m + M]$ which are taken into account. The output of the program gives the full solution at each iteration step, meaning the incident, reflected and transmitted modal amplitude vectors $\{a_m\}$, $\{b_m\}$ and $\{b_m\}$ for the incident azimuthal mode m together with the solution field $\{p_m\}$. Furthermore, it gives all solution fields $\{p_n\}$ and transmitted modal amplitude vectors $\{c_n\}$ for each non-incident azimuthal mode n at each iteration.

The user can choose between *Jacobi* and *Gauss-Seidel* iterations. *Jacobi* iterations means in this case that for a specific iteration i, the program solves for each $\{p_n\}$ using the vector $\{f_n\}$ calculated at iteration $i - 1$ (see equation 36). In case of *Gauss-Seidel* iterations, after solving for a specific $\{p_k\}$, $k \in [m - M, m + M]$, a new value for $\{f_n\}$ is calculated using all $\{p_n\}$, $n \leq k$. This new value for $\{f_n\}$ is then used when solving for $\{p_{k+1}\}$. The number of iterations n_{it} can be altered in the code of the function *Iterations 2D* and is standard set to 10.

7 Results 1D Eigenproblem

This section shows the result of the numerical Matlab solver to the one dimensional eigenproblem described in section 3. Solutions are calculated in a duct without any additional hard-walled inlet or outlet area ($x_1 = 0$ and $x_2 = L$ in figure 2), with $L = 1$ and $R = 1$. Results for a fully hard-walled duct ($A_2 = 0$ along Γ_{wall}) are compared with the exact solution described in the first part of this section. A lined case ($A_2 \neq 0$) is compared with reference values obtained from literature.

Exact solution

For a hard-walled, cyclindrical duct, the exact solution $p_{ex}(r)$ to equation 4 is a ordinary Bessel function of the first kind,

$$p_{ex}(r) = J_m(\alpha_{m\mu}\frac{r}{R}), \tag{38}$$

where m is the azimuthal mode order, $\mu = 1, 2, ...$ and $\alpha_{m\mu}$ is the μ-th non-negative zero of the derivative of the Bessel function, J'_m. Values for $\alpha_{m\mu}$ and $J_m(\alpha_{m\mu}r)$ at the duct center ($r = 0$) and duct wall ($r = R = 1$) are given for the first five values for μ in table 2. These values are used in the remainder of this section to validate the results of the numerical calculations for hard-walled cylindrical ducts.

Table 1: *First five exact solution values for a hard-walled, cylindrical duct for azimuthal modes $m = 0$, $m = 2$ and $m = 8$.*

	μ	$\alpha_{m\mu}$	$J_m(\alpha_{m\mu}r)\|_{r=0}$	$J_m(\alpha_{m\mu}r)\|_{r=1}$
$m = 0$	1	0	1	1
	2	3.8317	1	-0.4028
	3	7.0156	1	0.3001
	4	10.1735	1	-0.2497
	5	13.3237	1	0.2184
$m = 2$	1	3.0542	0	0.4865
	2	6.7061	0	-0.3135
	3	9.9695	0	0.2547
	4	13.1704	0	-0.2209
	5	16.3475	0	0.1979
$m = 8$	1	9.6474	0	0.3244
	2	14.1155	0	-0.2330
	3	17.7740	0	0.2000
	4	21.2291	0	-0.1798
	5	24.5872	0	0.1654

Axial wave number

Table 2 shows the first five eigenvalues $k\lambda$ for azimuthal modes $m = 0$, $m = 2$ and $m = 8$ for a hard walled, cylindrical duct of radius $R = 1$ with $k = 10$. The numerical values are obtained using a one dimensional mesh with respectively $N_r = 20$, $N_r = 100$ and $N_r = 200$ finite elements

in radial direction. The results show convergence to the exact solutions described above, where the eigenvalues $k\lambda$ are are calculated as

$$k\lambda = \sqrt{k^2 - \alpha_{m\mu}^2}. \tag{39}$$

Table 3 shows the first ten eigenvalues $k\lambda$ for azimuthal mode $m = 0$ in case of a lined, cylindrical duct of radius $R = 1$ with $k = 1$, where wall admittance $A_2 = 1 + 1\imath$. Again, numerical values are obtained using a one dimensional mesh with respectively $N_r = 20$, $N_r = 100$ and $N_r = 200$ finite elements in radial direction and just as in the hard-walled case, convergence to the reference values is observed. The reference values are in this case obtained by Vo and Eversman [5], using a Runge-Kutta integration scheme as comparison values to their method of weighted residuals.

Table 2: *First five exact and numerical eigenvalues $k\lambda$ for a hard-walled, cylindrical duct with $kR = 10$ for azimuthal modes $m = 0$, $m = 2$ and $m = 8$.*

	μ	Exact	FE method $N_r = 20$	FE method $N_r = 100$	FE method $N_r = 200$
$m = 0$	1	10.0000	10.0000	10.0000	10.0000
	2	9.2368	9.2352	9.2367	9.2368
	3	7.1261	7.0980	7.1250	7.1258
	4	$-1.8709i$	$-2.3254i$	$-1.8910i$	$-1.8758i$
	5	$-8.8046i$	$-9.1308i$	$-8.8178i$	$-8.8079i$
$m = 2$	1	9.5222	9.5219	9.5222	9.5222
	2	7.4181	7.4047	7.4175	7.4179
	3	0.7804	$-0.8026i$	0.7481	0.7728
	4	$-8.5708i$	$-8.8203i$	$-8.5809i$	$-8.5733i$
	5	$-12.9322i$	$-13.3559i$	$-12.9493i$	$-12.9365i$
$m = 8$	1	2.6320	2.6144	2.6313	2.6318
	2	$-9.9623i$	$-10.0310i$	$-9.9651i$	$-9.9630i$
	3	$-14.6940i$	$-14.8817i$	$-14.7017i$	$-14.6960i$
	4	$-18.7263i$	$-19.1131i$	$-18.7421i$	$-18.7302i$
	5	$-22.4618i$	$-23.1447i$	$-22.4898i$	$-22.4688i$

1D Pressure field

Figure 9 shows the shapes of the first five eigensolution fields $\{p_m\}_{norm}$ for azimuthal modes $m = 0$, $m = 2$ and $m = 8$ in a hard-walled, cylindrical duct of radius $R = 1$ with $kR = 10$, together with some exact values for comparison. The exact values are equal to the Bessel solutions 38 shown in table 1, normalized in the same way as the numerical solution fields according to equations 17 and 19, where the integral is numerically solved using a 64 point Gauss Quadrature for numerical integration. The computational results are obtained using a one dimensional grid with $N_r = 20$ finite elements in radial direction.

Figure 10 shows the real (left) and imaginary (right) parts of the normalized solution fields $\{p_m\}_{norm}$ for similar conditions in a lined cylindrical duct with $A_2 = 1 + 1\imath$, together with some exact values for comparison. The exact values are again equal to the Bessel solutions 38, where

Table 3: *First ten reference and numerical eigenvalues $k\lambda$ for a lined cylindrical duct with $kR = 1$ and admittance $A_2 = 1 + i$ for azimuthal mode $m = 0$.*

μ	Reference [5]	FE method $N_r = 20$	FE method $N_r = 100$	FE method $N_r = 200$
1	$1.880 - 0.845i$	$1.8798 - 0.8448i$	$1.8797 - 0.8450i$	$1.8797 - 0.8450i$
2	$0.278 - 3.414i$	$0.2793 - 3.4169i$	$0.2783 - 3.4142i$	$0.2783 - 3.4141i$
3	$0.145 - 6.798i$	$0.1471 - 6.8246i$	$0.1451 - 6.7990i$	$0.1451 - 6.7982i$
4	$0.099 - 10.025i$	$0.1022 - 10.1155i$	$0.0992 - 10.0284i$	$0.0991 - 10.0257i$
5	$0.075 - 13.211i$	$0.0795 - 13.4248i$	$0.0756 - 13.2192i$	$0.0755 - 13.2127i$
6	$0.061 - 16.379i$	$0.0661 - 16.7960i$	$0.0611 - 16.3960i$	$0.0610 - 16.3835i$
7	$0.051 - 19.539i$	$0.0574 - 20.2567i$	$0.0513 - 19.5680i$	$0.0511 - 19.5464i$
8	$0.044 - 22.694i$	$0.0515 - 23.8292i$	$0.0443 - 22.7397i$	$0.0441 - 22.7055i$
9	$0.039 - 25.846i$	$0.0474 - 27.5328i$	$0.0390 - 25.9136i$	$0.0387 - 25.8627i$
10	$0.034 - 28.995i$	$0.0446 - 31.3829i$	$0.0348 - 29.0916i$	$0.0346 - 28.0192i$

the values $\alpha_{m\mu}$ are obtained by substituting the numerically calculated eigenvalues $k\lambda$ into equation 39. The computational results are obtained using a one dimensional grid with $N_r = 20$ finite elements in radial direction.

As can be seen from tables 2 and 3, even for smaller grid sizes ($N_r = 20$), the eigenvalues are comparable to the exact values and convergence to these exact values is observed as the computational grid gets finer. For higher modes ν, the deviation from the exact values gets larger. The same is observed for the normalized eigenvectors $\{p_m\}_{norm}$ in figures 9 and 10, where higher modes ν show more deviation from the exact values than the lower modes. Also, for the lined case in figure 10, the deviation from the exact values is higher for the imaginary part of the solution than for the real part.

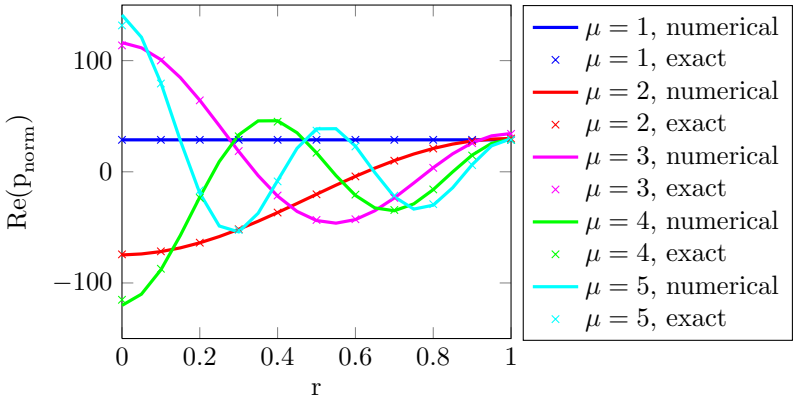

(a) $m = 0$

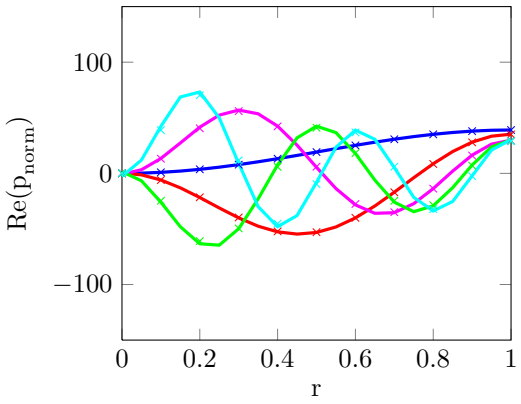

(b) $m = 2$

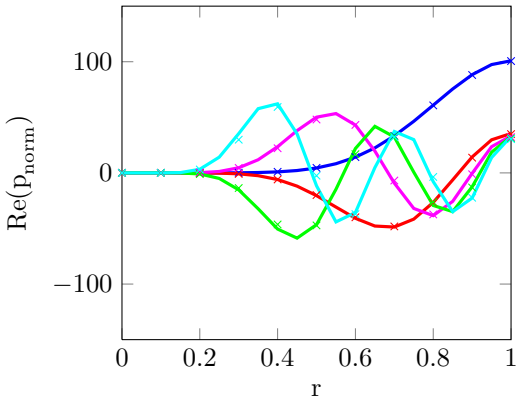

(c) $m = 8$

Figure 9: Plots of the first five computational and exact solutions to the 1D eigenproblem for a uniform hard-walled circular duct with $kR = 10$ and different values for m, calculated on a grid of $N_r = 20$.

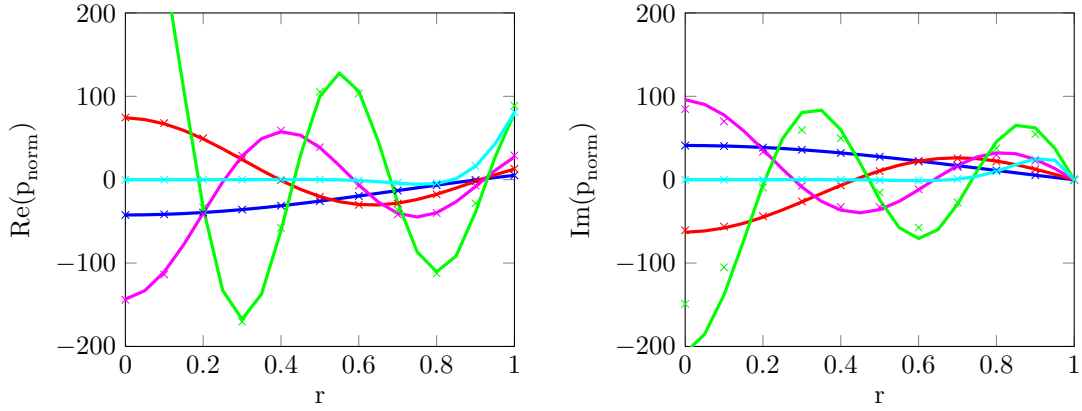

(a) $m = 0$, real part

(b) $m = 0$, imaginary part

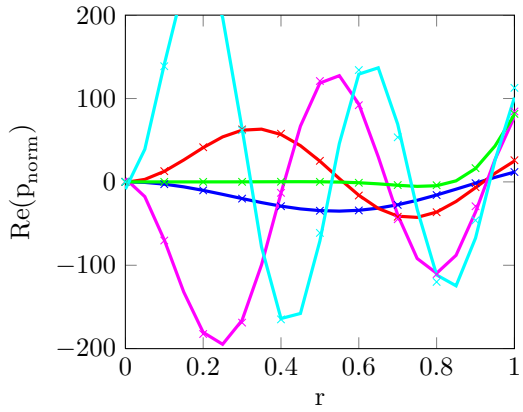

(c) $m = 2$, real part

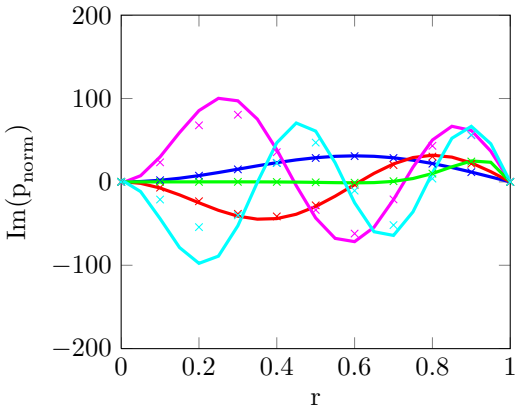

(d) $m = 2$, imaginary part

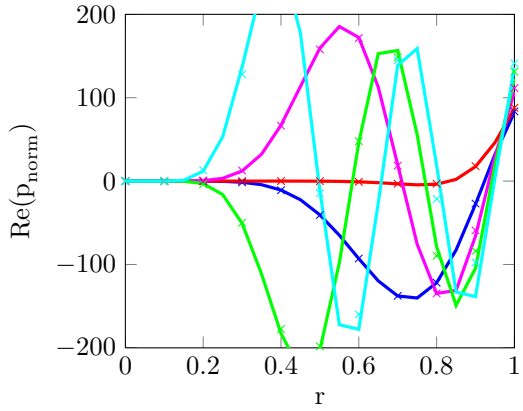

(e) $m = 8$, real part

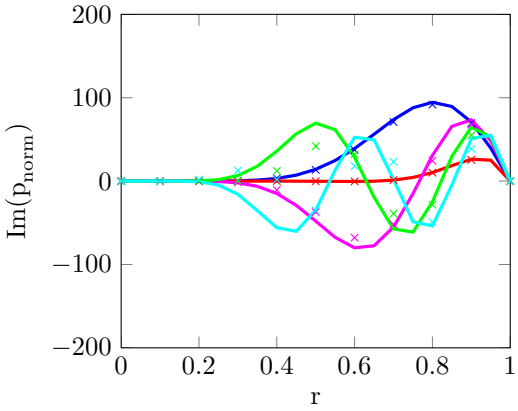

(f) $m = 8$, imaginary part

Figure 10: Plots of the first five computational and exact solutions to the 1D eigenproblem for a uniform lined circular duct with $kR = 10$, $A_1 = 0$, $A_2 = 1 + \imath$ and different values for m, calculated on a grid of $N_r = 20$. Colorscheme/legend equal to figure 9.

8 Results 2D Transmission in axisymmetric lined ducts

This section shows the results of the numerical Matlab solver to the two dimensional sound transmission problem described in section 4. Solutions are calculated in a duct without any additional hard-walled inlet or outlet area ($x_1 = 0$ and $x_2 = L$ in figure 2), with $L = 1$ and $R = 1$. The results for hard-walled ducts are compared with exact transmission solutions described in the first part of this section. In the second part, results for a lined case are validaded based on the modal amplitudes of the incident, reflected and transmitted modes.

As described in section 6, the Matlab code on solving the 2D Transmission problem lets the user define the number of 1D eigensolutions, i.e. the number of radial modes, which are matched to the 2D problem and used for the evaluation of the stiffness matrices according to equations 25. All results on this section on the results for axisymmetric lining and in the next section on the results for non-axisymmetric lining are obtained by taking $n_\mu = 5$ radial modes into account for each azimuthal mode m. Table 4 shows the numerically calculated eigenvalues $k\lambda$ for the first five radial modes for each of the three azimuthal mode m cases of which the results are presented in this report. As can be seen, in every case all cut on modes (with real values for $k\lambda$ in the hard-walled case) and at least two cut-off modes are taken into account.

Table 4: *First five numericaly calculated eigenvalues $k\lambda$ at a grid size $N_r = 20$ for a hard-walled ($A_2 = 0$) and a lined ($A_2 = 1 + 1\imath$) cylindrical duct with $kR = 10$ for azimuthal modes $m = 0$, $m = 2$ and $m = 8$, and the values $e^{-\imath k\lambda_{m\mu}L}$ for these specific modes at $L = 1$.*

	μ	$k\lambda_{m\mu}$, Hard-walled	$e^{-\imath k\lambda_{m\mu}L}$, Hard-walled	$k\lambda_{m\mu}$, lined	$e^{-\imath k\lambda_{m\mu}L}$, lined
$m = 0$	1	10.0000	$-0.8391 + 0.5440i$	$9.6764 - 0.0327i$	$-0.9373 + 0.2409i$
	2	9.2352	$-0.9821 - 0.1884i$	$8.1347 - 0.1981i$	$-0.2273 - 0.7882i$
	3	7.0980	$0.6860 - 0.7276i$	$4.0379 - 0.9025i$	$-0.2533 + 0.3168i$
	4	$-2.3254i$	0.0977	$0.7504 - 7.7591i$	$0.0003 - 0.0003i$
	5	$-9.1308i$	0.0001	$13.4056 - 7.8065i$	$0.0003 - 0.0003i$
$m = 2$	1	9.5219	$-0.9953 + 0.0970i$	$8.4167 - 0.1673i$	$-0.4513 - 0.7155i$
	2	7.4047	$0.4343 - 0.9008i$	$4.5939 - 0.7579i$	$-0.0554 + 0.4654i$
	3	$-0.8026i$	0.4482	$0.7733 - 7.3787i$	$0.0004 - 0.0004i$
	4	$-8.8203i$	0.0001	$13.2923 - 7.8812i$	$0.0003 - 0.0003i$
	5	$-13.3559i$	0.0000	$0.6100 - 12.3916i$	$0.0000 - 0.0000i$
$m = 8$	1	2.6144	$-0.8642 - 0.5031i$	$0.8337 - 8.2427i$	$(0.1769 - 0.1949i) \cdot 10^{-3}$
	2	$-10.0310i$	0.0000	$11.6311 - 9.1495i$	$(0.0631 + 0.0855i) \cdot 10^{-3}$
	3	$-14.8817i$	0.0000	$0.6467 - 13.8348i$	$(0.0008 - 0.0006i) \cdot 10^{-3}$
	4	$-19.1131i$	0.0000	$0.5522 - 18.3436i$	$(0.0000 - 0.0000i) \cdot 10^{-3}$
	5	$-23.1447i$	0.0000	$0.4895 - 22.5185i$	$(0.0000 - 0.0000i) \cdot 10^{-3}$

Table 4 furthermore shows the values for $e^{-\imath k\lambda_{m\mu}L}$ for each considered combination of azimuthal and radial mode. When injecting a specific incident mode (m, μ) with amplitude a_μ, the transmitted modal amplitude at the outlet of the duct should be equal to $a_\mu e^{-\imath k\lambda_{m\mu}L}$ in case of axisymmetric lining, where there is no scattering so that the transmitted modes should be similar to the injected modes.

Hard-walled duct

Table 5 shows the reflected and transmitted modal wave amplitudes $\{b\}$ and $\{c\}$ for a hard-walled duct and different azimuthal mode numbers m and incident modal amplotude vectors $\{a\}$. In each case, only one radial mode μ with amplitude $a_\mu = 1$ is injected. The numerical calculations are executed on a grid of size $N_x = N_r = 20$. The transmitted mode amplitudes $\{c\}$ show agreement with the 'exact' transmission values in table 4, where c_μ converges to $a_\mu e^{-\imath k \lambda_{m\mu} L}$ for the incident mode and all other components of $\{c\}$ converge to zero.

Table 5: *Reflected and transmitted mode vectors $\{b\}$ and $\{c\}$ for a specific incident mode vectors $\{a\}$ and azimuthal mode m, hard-walled duct, $kR = 10$, computations on grid size $N_x = N_r = 20$.*

	$\{a\}$	$\{b\}$	$\{c\}$
$m = 0$	1	$0.0018 + 0.0043i$	$-0.8894 + 0.4562i$
	0	$0.0011 - 0.0000i$	$-0.0010 - 0.0003i$
	0	$-0.0017 - 0.0000i$	$-0.0012 + 0.0012i$
	0	$0.0000 + 0.0075i$	$-0.0000 + 0.0007i$
	0	$-0.0000 - 0.0022i$	$0.0000 - 0.0000i$
$m = 0$	0	$-0.0012 - 0.0000i$	$0.0010 - 0.0005i$
	0	$0.0031 - 0.0000i$	$-0.0029 - 0.0008i$
	1	$-0.0021 + 0.0026i$	$0.7089 - 0.6986i$
	0	$0.0000 + 0.0211i$	$0.0000 + 0.0021i$
	0	$-0.0000 - 0.0063i$	$-0.0000 - 0.0000i$
$m = 0$	0	$-0.0000 + 0.0017i$	$-0.0008 - 0.0015i$
	0	$-0.0000 - 0.0045i$	$-0.0012 + 0.0044i$
	0	$-0.0000 + 0.0070i$	$0.0049 + 0.0050i$
	0	$0.0312 + 0.0000i$	$0.0030 - 0.0000i$
	1	$-0.0136 + 0.0000i$	$0.0001 - 0.0000i$
$m = 2$	1	$(0.0085 + 0.9012i) \cdot 10^{-4}$	$-1.0000 + 0.0095i$
	0	$(-0.0092 + 0.0053i) \cdot 10^{-4}$	$-0.0000 + 0.0000i$
	0	$(-0.0377 + 0.4590i) \cdot 10^{-4}$	$0.0000 + 0.0000i$
	0	$(0.0302 - 0.0320i) \cdot 10^{-4}$	$-0.0000 - 0.0000i$
	0	$(-0.0335 + 0.0231i) \cdot 10^{-4}$	$0.0000 + 0.0000i$
$m = 8$	1	$(0.1815 - 0.3104i) \cdot 10^{-3}$	$-0.8633 - 0.5047i$
	0	$(0.0000 - 0.0000i) \cdot 10^{-3}$	$-0.0000 - 0.0000i$
	0	$(0.0000 - 0.0000i) \cdot 10^{-3}$	$-0.0000 - 0.0000i$
	0	$(0.0000 - 0.0000i) \cdot 10^{-3}$	$-0.0000 - 0.0000i$
	0	$(-0.0000 + 0.0000i) \cdot 10^{-3}$	$0.0000 + 0.0000i$
$m = 8$	0	$0.0000 + 0.0000i$	$(0.0004 - 0.0005i) \cdot 10^{-10}$
	0	$0.0000 + 0.0000i$	$(0.0000 + 0.0000i) \cdot 10^{-10}$
	0	$-0.0000 + 0.0000i$	$(-0.0000 + 0.0000i) \cdot 10^{-10}$
	0	$0.0000 + 0.0000i$	$(0.0000 + 0.0000i) \cdot 10^{-10}$
	1	$-0.0264 + 0.0000i$	$(0.1937 + 0.0000i) \cdot 10^{-10}$

Figure 11 shows the variation of the sound pressure along the x-axis at both the centre of the duct at $x = 0$ and at the duct wall where $x = R$ for a hard walled duct with $A_1 = A_2 = 0$ and azimuthal mode $m = 0$. Some exact values are shown as well, which are equal to

$$p_{ex,norm} \cdot e^{-\imath k \lambda x} \tag{40}$$

with $p_{ex,norm}$ equal to the normalized Bessel solutions of equation 38 and $k\lambda$ equal to the exact values for the axial wave number computed according to equation 39. The computational results are obtained using a grid of size $N_x = N_r = 20$ elements. Figure 12 shows on the left hand side the variation of the sound pressure along the x-axis at the duct wall for several cases with $m \neq 0$ in a hard-walled duct, also calculated on a $N_x = N_r = 20$ grid. In all cases, good agreement with the exact hard-walled results is found.

Lined duct

Table 6 shows the reflected and transmitted modal wave amplitudes $\{b\}$ and $\{c\}$ for a lined duct, $A_2 = 1 + \imath$, and different azimuthal mode numbers m and incident modal amplotude vectors $\{a\}$. Numerical calculations are done on a $N_x = N_r = 50$ grid. Just as for the hard-walled case, agreement is found between the numerical calculated transmitted modal amplitudes $\{c\}$ and the 'exact' values in table 4. Figure 12 shows on the right hand side the solution fields at the duct wall in case of the lined duct under similar circumstances as the hard-walled cases on the left hand side. It shows similar wave solutions, differing only in amplitude and rate of attenuation.

Table 6: *Reflected and transmitted mode vectors $\{b\}$ and $\{c\}$ for a specific incident mode vectors $\{a\}$ and azimuthal mode m, lined duct with $A_1 = 0$ and $A_2 = 1 + 1\imath$, $kR = 10$, computations on grid size $N_x = N_r = 50$.*

	$\{a\}$	$\{b\}$	$\{c\}$
$m = 0$	1	$(-0.1409 + 0.3059i) \cdot 10^{-3}$	$-0.9407 + 0.2269i$
	0	$(0.4697 + 0.0201i) \cdot 10^{-3}$	$-0.0001 - 0.0004i$
	0	$(-0.8347 - 0.0746i) \cdot 10^{-3}$	$0.0002 - 0.0003i$
	0	$(0.0855 + 0.2193i) \cdot 10^{-3}$	$0.0000 + 0.0000i$
	0	$(-0.0001 + 0.0001i) \cdot 10^{-3}$	$-0.0000 + 0.0000i$
$m = 0$	0	$(-0.3347 - 0.0261i) \cdot 10^{-3}$	$0.0003 - 0.0001i$
	0	$(0.5754 + 0.0127i) \cdot 10^{-3}$	$-0.0001 - 0.0005i$
	1	$(-0.8662 - 0.1114i) \cdot 10^{-3}$	$-0.2278 + 0.3580i$
	0	$(0.1102 + 0.2662i) \cdot 10^{-3}$	$0.0000 + 0.0000i$
	0	$(-0.0001 + 0.0001i) \cdot 10^{-3}$	$-0.0000 + 0.0000i$
$m = 2$	1	$(0.7644 - 0.4109i) \cdot 10^{-3}$	$-0.4466 - 0.7197i$
	0	$(-0.0001 - 0.0001i) \cdot 10^{-3}$	$-0.0000 - 0.0000i$
	0	$(-0.0001 + 0.0001i) \cdot 10^{-3}$	$-0.0000 + 0.0000i$
	0	$(-0.0000 - 0.0000i) \cdot 10^{-3}$	$-0.0000 - 0.0000i$
	0	$(0.0001 - 0.0001i) \cdot 10^{-3}$	$-0.0000 - 0.0000i$
$m = 8$	1	$(-0.5562 - 0.1131i) \cdot 10^{-3}$	$(0.1807 - 0.1979i) \cdot 10^{-3}$
	0	$(0.0000 - 0.0000i) \cdot 10^{-3}$	$(0.0000 + 0.0000i) \cdot 10^{-3}$
	0	$(-0.0000 + 0.0000i) \cdot 10^{-3}$	$(0.0000 + 0.0000i) \cdot 10^{-3}$
	0	$(0.0000 - 0.0000i) \cdot 10^{-3}$	$(0.0000 - 0.0000i) \cdot 10^{-3}$
	0	$(0.0000 - 0.0000i) \cdot 10^{-3}$	$(-0.0000 - 0.0000i) \cdot 10^{-3}$
$m = 8$	0	$0.0000 + 0.0000i$	$(0.0000 - 0.0000i) \cdot 10^{-9}$
	0	$0.0000 - 0.0000i$	$(-0.0000 - 0.0000i) \cdot 10^{-9}$
	0	$0.0000 + 0.0000i$	$(-0.0000 - 0.0000i) \cdot 10^{-9}$
	0	$0.0000 + 0.0000i$	$(0.0000 - 0.0000i) \cdot 10^{-9}$
	1	$-0.0040 - 0.0002i$	$(0.2061 - 0.1014i) \cdot 10^{-9}$

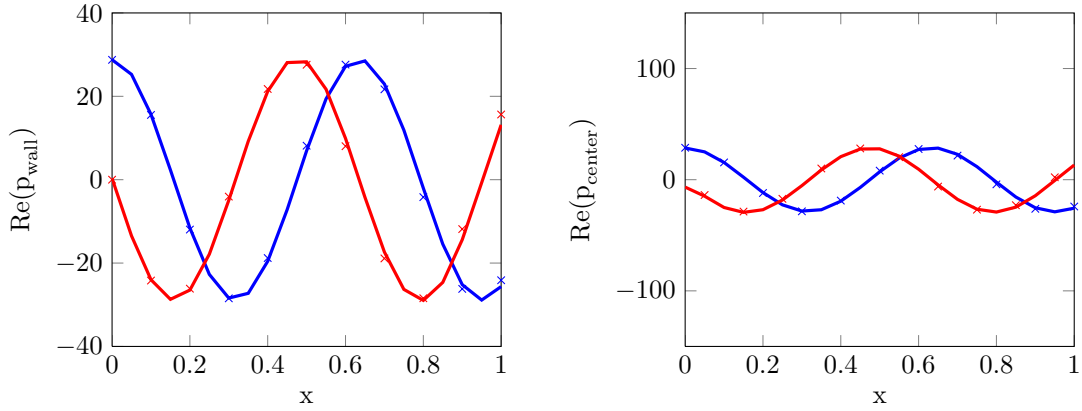

(a) $m = 0$, $\mu = 1$, wall

(b) $m = 0$, $\mu = 1$, center

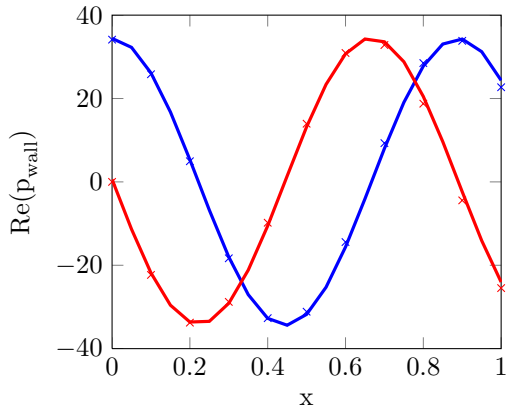

(c) $m = 0$, $\mu = 3$, wall

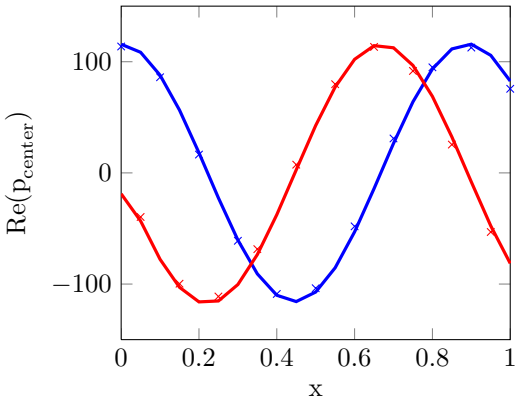

(d) $m = 0$, $\mu = 3$, center

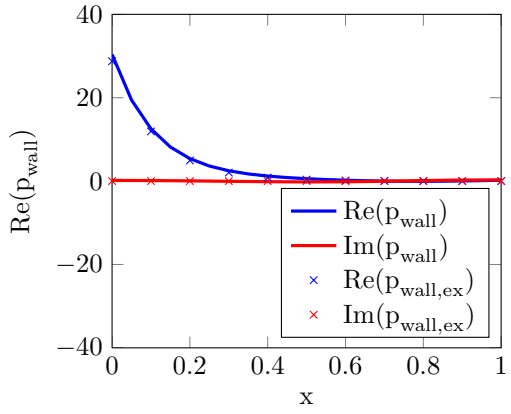

(e) $m = 0$, $\mu = 5$, wall

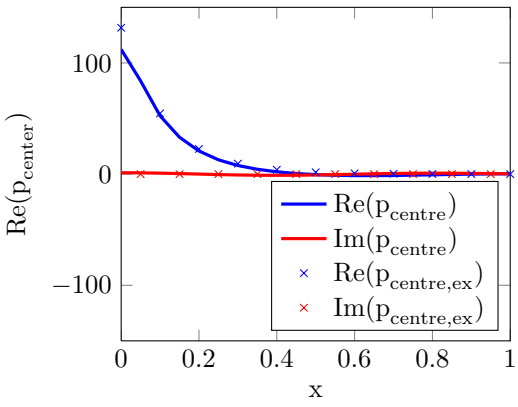

(f) $m = 0$, $\mu = 5$, center

Figure 11: Plots of the real and imaginary parts of the computational and exact solutions to the 2D transmission problem for a uniform hard-walled circular duct with $kR = 10$, $m = 0$ and different incident modes μ, calculated on a grid of $N_x = N_r = 20$.

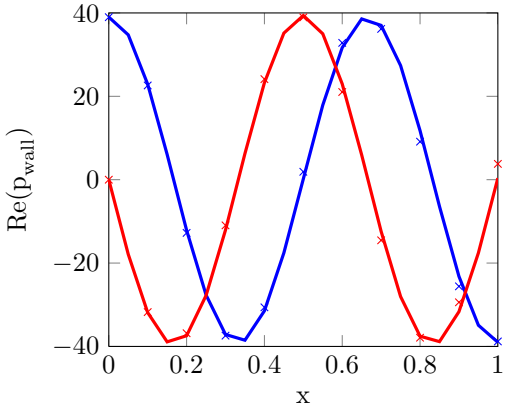

(a) $m = 2$, $\mu = 1$, wall, hard-walled

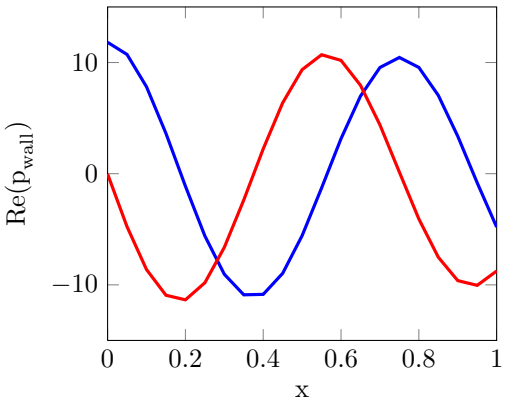

(b) $m = 2$, $\mu = 1$, wall, lined

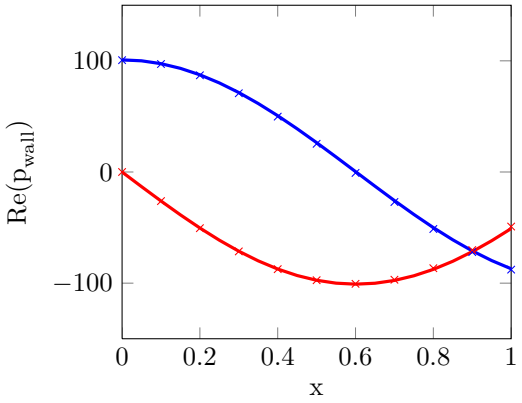

(c) $m = 8$, $\mu = 1$, wall, hard-walled

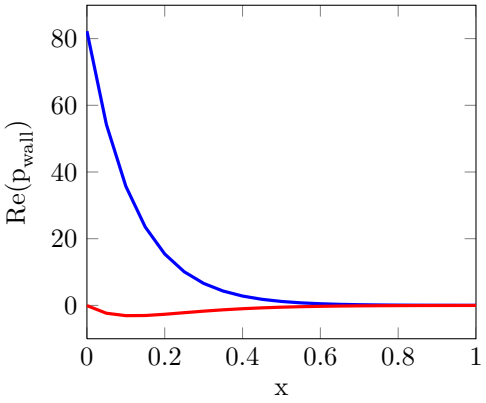

(d) $m = 8$, $\mu = 1$, wall, lined

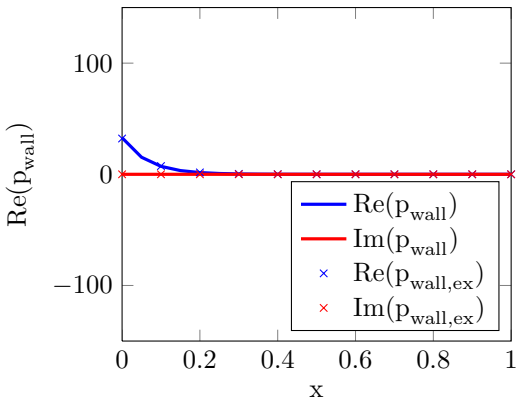

(e) $m = 8$, $\mu = 5$, wall, hard-walled

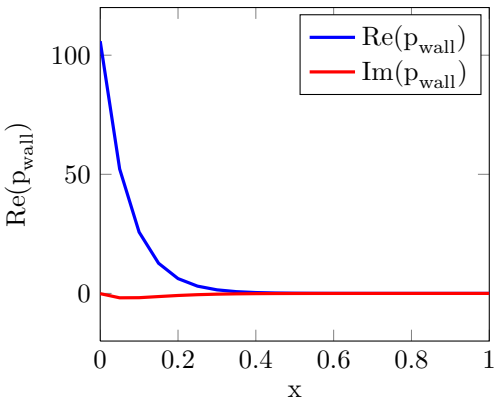

(f) $m = 8$, $\mu = 5$, wall, lined

Figure 12: Plots of the real and imaginary parts of the computational solutions to the 2D transmission problem at the duct wall for a uniform hard-walled circular duct (left) and a lined duct with $A_2 = 1 + 1\imath$ (right) with $kR = 10$ and different incident modes m and μ, calculated on a grid of $N_x = N_r = 20$. For the hard-walled duct, some exact solutions are shown as well.

9 Results 2D Transmission in non-axisymmetric lined ducts

The iterative method for sound transmission in non-axisymmetric lined ducts is tested on two cases of similar duct geometry and incident mode specifications, differing in the type of liner discontinuity. In case 1, the lining is non-axisymmetric due to the presence of a liner splice over the full length of the liner; in case 2, the lining is non-axisymmetric due to a small patch of damage/repair in the lining at a certain position. This section will describe both cases in more detail and will discuss the results that have obtained from the Matlab code so far.

Case 1: liner splice

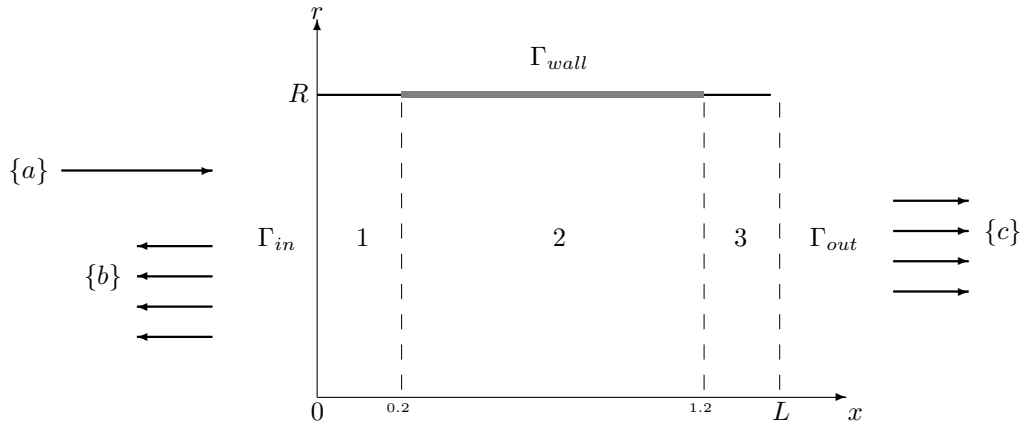

Figure 13: Duct geometry and different lined sections.

Total duct: Length $L = 1.4$, constant radius $R = 1$, structured mesh with number of elements in x-direction $N_x = 28$ and in r-direction $N_r = 20$.

Section 1: axi-symmetric hard-walled inlet area from $x = 0$ to $x = 0.2$ ($N_x = 4$, $N_r = 20$). Impedance $A_1 = 0$ (at $x = 0$), $A_2 = 0$ (at $x = R$).

Section 2: Lined duct area with hard-walled splice for $-\frac{pi}{32} \leq \theta \leq \frac{pi}{32}$ from $x = 0.2$ to $x = 1.2$ ($N_x = 20$, $N_r = 20$). Impedance $A_1 = 0$ (at $x = 0$), $A_2 = 1 + 1\imath$ (at $x = R$). Splice impedance $A_s = 0$.

Section 3: axi-symmetric hard-walled inlet area from $x = 1.2$ to $x = 1.4$ ($N_x = 4$, $N_r = 20$). Impedance $A_1 = 0$ (at $x = 0$), $A_2 = 0$ (at $x = R$).

Problem details: No flow, wave number $kR = 10$, incident azimuthal mode $m = 0$, incident radial mode $\mu = 1$, azimuthal scattered mode range $n \in [m - M, m + M]$ with $M = 10$, first 5 radial modes for each mode n taken into account.

Table 7 shows the reflected and transmitted modal amplitudes for all five radial modes μ for the incident azimuthal mode m, in case 1 after each iteration.

(a) *Reflected mode vectors $b_{0,\mu}$ for case 1, iterations 1 to 8*

$b_{0,\mu}$	iteration 1	iteration 2	iteration 3	iteration 4
$b_{0,1}$	$-0.0238 - 0.0310i$	$0.0084 - 0.0095i$	$0.0168 - 0.0046i$	$0.0209 - 0.0037i$
$b_{0,2}$	$-0.0133 - 0.0407i$	$0.0053 - 0.0153i$	$0.0171 - 0.0206i$	$0.0314 - 0.0227i$
$b_{0,3}$	$-0.0373 - 0.0292i$	$0.0235 - 0.0217i$	$0.0772 + 0.0178i$	$0.0893 + 0.0581i$
$b_{0,4}$	$0.0137 + 0.1725i$	$0.0254 + 0.0301i$	$0.0412 - 0.0332i$	$0.0656 - 0.0679i$
$b_{0,5}$	$-0.0050 + 0.0074i$	$-0.0014 - 0.0023i$	$0.0012 - 0.0046i$	$0.0023 - 0.0049i$

$b_{0,\mu}$	iteration 5	iteration 6	iteration 7	iteration 8
$b_{0,1}$	$0.0238 - 0.0006i$	$0.0228 + 0.0047i$	$0.0175 + 0.0078i$	$0.0122 + 0.0058i$
$b_{0,2}$	$0.0398 - 0.0151i$	$0.0370 - 0.0053i$	$0.0270 - 0.0026i$	$0.0195 - 0.0086i$
$b_{0,3}$	$0.0777 + 0.0773i$	$0.0641 + 0.0763i$	$0.0594 + 0.0653i$	$0.0653 + 0.0550i$
$b_{0,4}$	$0.0931 - 0.0767i$	$0.1108 - 0.0672i$	$0.1132 - 0.0523i$	$0.1041 - 0.0440i$
$b_{0,5}$	$0.0026 - 0.0050i$	$0.0029 - 0.0051i$	$0.0031 - 0.0050i$	$0.0032 - 0.0047i$

(b) *Transmitted mode vectors $c_{0,\mu}$ for case 1, iterations 1 to 8*

$c_{0,\mu}$	iteration 1	iteration 2	iteration 3	iteration 4
$c_{0,1}$	$0.3729 - 0.5385i$	$0.3033 - 0.5064i$	$0.2466 - 0.5167i$	$0.2008 - 0.5449i$
$c_{0,2}$	$-0.1617 + 0.3642i$	$-0.1678 + 0.3910i$	$-0.1895 + 0.3859i$	$-0.2149 + 0.3641i$
$c_{0,3}$	$-0.1422 - 0.2087i$	$-0.2978 - 0.0066i$	$-0.3870 + 0.0149i$	$-0.4216 - 0.0109i$
$c_{0,4}$	$0.0351 - 0.1595i$	$0.1578 + 0.0560i$	$0.0963 + 0.1149i$	$0.0796 + 0.0879i$
$c_{0,5}$	$0.0002 - 0.0069i$	$0.0049 - 0.0019i$	$0.0034 - 0.0013i$	$0.0038 - 0.0029i$

$c_{0,\mu}$	iteration 5	iteration 6	iteration 7	iteration 8
$c_{0,1}$	$0.1742 - 0.5905i$	$0.1802 - 0.6383i$	$0.2110 - 0.6634i$	$0.2408 - 0.6589i$
$c_{0,2}$	$-0.2282 + 0.3259i$	$-0.2150 + 0.2873i$	$-0.1830 + 0.2710i$	$-0.1565 + 0.2812i$
$c_{0,3}$	$-0.4217 - 0.0451i$	$-0.3969 - 0.0668i$	$-0.3669 - 0.0626i$	$-0.3538 - 0.0404i$
$c_{0,4}$	$0.1067 + 0.0847i$	$0.1168 + 0.1133i$	$0.0979 + 0.1337i$	$0.0766 + 0.1297i$
$c_{0,5}$	$0.0058 - 0.0028i$	$0.0065 - 0.0009i$	$0.0054 + 0.0006i$	$0.0040 + 0.0005i$

Table 7: Reflected and transmitted mode amplitudes for incident azimuthal mode m, case 1.

Case 2: patch

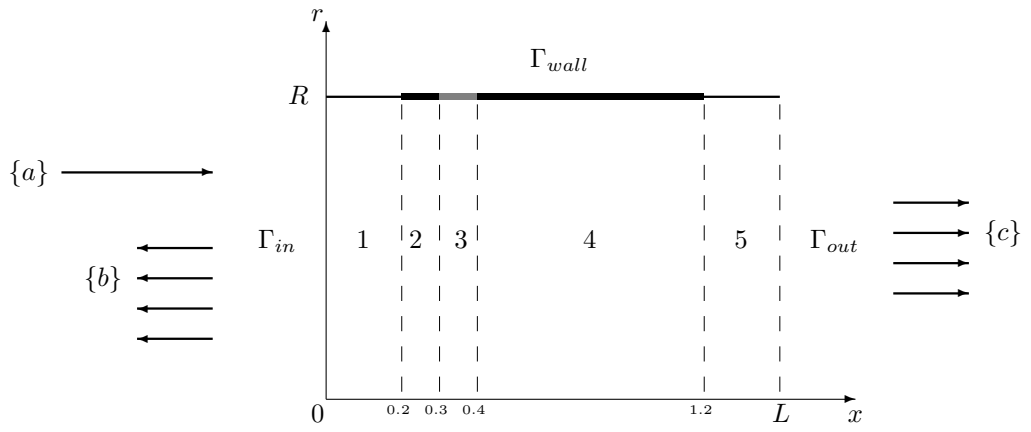

Figure 14: Duct geometry and different lined sections.

Total duct: Length $L = 1.4$, constant radius $R = 1$, structured mesh with number of elements in x-direction $N_x = 28$ and in r-direction $N_r = 20$.

Section 1: axi-symmetric hard-walled inlet area from $x = 0$ to $x = 0.2$ ($N_x = 4$, $N_r = 20$). Impedance $A_1 = 0$ (at $x = 0$), $A_2 = 0$ (at $x = R$).

Section 2: axi-symmetric lined duct area from $x = 0.2$ to $x = 0.3$ ($N_x = 2$, $N_r = 20$). Impedance $A_1 = 0$ (at $x = 0$), $A_2 = 1 + 1\imath$ (at $x = R$).

Section 3: Lined duct area with hard-walled patch for $-\frac{pi}{32} \leq \theta \leq \frac{pi}{32}$ from $x = 0.3$ to $x = 0.4$ ($N_x = 2$, $N_r = 20$). Impedance $A_1 = 0$ (at $x = 0$), $A_2 = 1 + 1\imath$ (at $x = R$). Patch impedance $A_p = 0$.

Section 4: axi-symmetric lined duct area from $x = 0.4$ to $x = 1.2$ ($N_x = 16$, $N_r = 20$). Impedance $A_1 = 0$ (at $x = 0$), $A_2 = 1 + 1\imath$ (at $x = R$).

Section 5: axi-symmetric hard-walled inlet area from $x = 1.2$ to $x = 1.4$ ($N_x = 4$, $N_r = 20$). Impedance $A_1 = 0$ (at $x = 0$), $A_2 = 0$ (at $x = R$).

Problem details: No flow, wave number $kR = 10$, incident azimuthal mode $m = 0$, incident radial mode $\mu = 1$, azimuthal scattered mode range $n \in [m - M, m + M]$ with $M = 10$, first 5 radial modes for each mode n taken into account.

Table 8 shows the reflected and transmitted modal amplitudes for all five radial modes μ for the incident azimuthal mode m, in case 2 after each iteration.

(a) *Reflected mode vectors $b_{0,\mu}$ for case 2, iterations 1 to 8*

$b_{0,\mu}$	iteration 1	iteration 2	iteration 3	iteration 4
$b_{0,1}$	$-0.0249 - 0.0320i$	$-0.0196 - 0.0876i$	$0.0030 - 0.0991i$	$0.0119 - 0.0926i$
$b_{0,2}$	$-0.0142 - 0.0422i$	$0.0027 - 0.0942i$	$0.0268 - 0.1003i$	$0.0339 - 0.0923i$
$b_{0,3}$	$-0.0373 - 0.0302i$	$0.0155 - 0.0681i$	$0.0417 - 0.0569i$	$0.0425 - 0.0448i$
$b_{0,4}$	$0.0144 + 0.1767i$	$-0.0530 + 0.1782i$	$-0.0676 + 0.1561i$	$-0.0625 + 0.1463i$
$b_{0,5}$	$-0.0050 + 0.0076i$	$-0.0061 + 0.0079i$	$-0.0065 + 0.0078i$	$-0.0065 + 0.0076i$

$b_{0,\mu}$	iteration 5	iteration 6	iteration 7	iteration 8
$b_{0,1}$	$0.0111 - 0.0881i$	$0.0093 - 0.0875i$	$0.0087 - 0.0881i$	$0.0088 - 0.0884i$
$b_{0,2}$	$0.0321 - 0.0881i$	$0.0303 - 0.0879i$	$0.0299 - 0.0886i$	$0.0300 - 0.0889i$
$b_{0,3}$	$0.0381 - 0.0422i$	$0.0364 - 0.0434i$	$0.0365 - 0.0443i$	$0.0368 - 0.0444i$
$b_{0,4}$	$-0.0578 + 0.1464i$	$-0.0570 + 0.1481i$	$-0.0575 + 0.1488i$	$-0.0578 + 0.1487i$
$b_{0,5}$	$-0.0064 + 0.0075i$	$-0.0064 + 0.0075i$	$-0.0064 + 0.0075i$	$-0.0064 + 0.0075i$

(b) *Transmitted mode vectors $c_{0,\mu}$ for case 2, iterations 1 to 8*

$c_{0,\mu}$	iteration 1	iteration 2	iteration 3	iteration 4
$c_{0,1}$	$0.3766 - 0.5396i$	$0.3580 - 0.5353i$	$0.3536 - 0.5410i$	$0.3549 - 0.5436i$
$c_{0,2}$	$-0.1593 + 0.3652i$	$-0.1593 + 0.3627i$	$-0.1585 + 0.3626i$	$-0.1583 + 0.3628i$
$c_{0,3}$	$-0.1422 - 0.2106i$	$-0.1535 - 0.1535i$	$-0.1757 - 0.1478i$	$-0.1818 - 0.1547i$
$c_{0,4}$	$0.0319 - 0.1601i$	$0.0534 - 0.1155i$	$0.0417 - 0.0998i$	$0.0338 - 0.1012i$
$c_{0,5}$	$0.0000 - 0.0069i$	$0.0013 - 0.0060i$	$0.0013 - 0.0054i$	$0.0010 - 0.0053i$

$c_{0,\mu}$	iteration 5	iteration 6	iteration 7	iteration 8
$c_{0,1}$	$0.3560 - 0.5437i$	$0.3563 - 0.5432i$	$0.3562 - 0.5431i$	$0.3561 - 0.5431i$
$c_{0,2}$	$-0.1584 + 0.3630i$	$-0.1584 + 0.3629i$	$-0.1584 + 0.3629i$	$-0.1584 + 0.3629i$
$c_{0,3}$	$-0.1804 - 0.1583i$	$-0.1788 - 0.1584i$	$-0.1784 - 0.1579i$	$-0.1786 - 0.1576i$
$c_{0,4}$	$0.0328 - 0.1044i$	$0.0338 - 0.1053i$	$0.0344 - 0.1051i$	$0.0344 - 0.1049i$
$c_{0,5}$	$0.0009 - 0.0054i$	$0.0009 - 0.0054i$	$0.0010 - 0.0054i$	$0.0010 - 0.0054i$

Table 8: Reflected and transmitted mode amplitudes for incident azimuthal mode m, case 2.

Discussion

The results in tables 7 and 8 show convergence in the modal amplitudes of the reflected and transmitted modes within the iterative process. They also show that the rate of convergence depends on the size of the liner discontinuity, as the results for the small patch (case 2) seem to converge faster than the results for the splice over the full length of the lining (case 1).

Furthermore, considering the method as described in section 5, after the first iteration the results in both cases should be similar to the results of the 2D transmission problem for a similar duct in absence of any liner discontinuity. Table 9 shows the results for the 2D transmission problem of a duct similar in geometry and in similar conditions as case 1 and 2, in absence of any liner discontinuity as a splice or patch. As can be seen, the results for the non-axisymmetric lined ducts after 1 iteration and the results for the axisymmetric lined ducts are comparable, differing from each other slightly due to the change in numerical calculations.

Table 9: *Reflected and transmitted mode vectors* $\{b\}$ *and* $\{c\}$ *for specific incident radial mode* $a_1 = 1$ *and azimuthal mode* $m = 0$ *in case of a duct similar in geometry to case 1 and 2, in absence of any liner discontinuity.*

$\{a\}$	$\{b\}$	$\{c\}$
1	$-0.0244 - 0.0306i$	$0.3770 - 0.5399i$
0	$-0.0140 - 0.0407i$	$-0.1593 + 0.3652i$
0	$-0.0381 - 0.0287i$	$-0.1426 - 0.2121i$
0	$0.0161 + 0.1759i$	$0.0309 - 0.1610i$
0	$-0.0050 + 0.0076i$	$-0.0000 - 0.0069i$

A way to validate the inclusion of the lining discontinuities is by looking at the results after the second iteration, where the effect of the non-axisymmetric lining is first taken into the equations. These results can be compared with the results for similar duct geometries and incident modes using the Cargill code developed by Cargill and improved by Brian Tester. The Cargill code uses a similar semi-analytical model for the 2D sound progapation as described in this report, but is not extended with the iterative model for non-symmetric lining. Including a lining discontinuity such as a splice or patch to the Cargill code model should therefore give results equal to the results after the second iteration of the method described in this report [11].

For the two test cases described in this section, Brian Tester has provided data such as the pressure distribution along the duct wall and the powerlevel in the duct as a function of x for all modes n obtained using the Cargill code. At the moment of writing however, no agreement between the two different codes has been found yet, suggesting there are still (erroneous) discrepancies present between the two codes.

10 Conclusions and future work

Conclusions

A full Matlab code has been developed to solve the sound transmission in a circular duct in absence of flow, attenuated by a non-axisymmetric lined duct surface with patches or splices. The code is a complete finite element solver, from creating a computational grid based on geometry specifications of the duct to solving the problem based on the parameters that come with it, solving the three main sub-problems on its way;

- The 1D eigenproblem for radial modes at inlet and outlet of the duct,
- The 2D transmission problem for axisymmetric lined ducts for a specific incidemt azimuthal mode m,
- The 2D transmission problem for non-axisymmetric lined ducts, coupeling the equations for incident azimuthal mode m and scattered azimuthal modes n.

The results for the 1D eigenproblem and the 2D transmission problem for axisymmetric lined ducts have been validated against exact results or results obtained from literature. The results from the iterative method to solve for non-axisymmetric lining are proved to be converging to a specific solution, which is promising for the validation of the method. Comparing the results with those of an existing method (Cargill code) however, has not yet revealed any agreement, suggesting there are still (errorenous) discrepanties between the two codes and improvement of the code presented in this report is still necessary.

Future work

As said, the results obtained using the iterative method for non-axisymmetric lined ducts so far are yet to be positively validated against other existing methods. The comparison with the Cargill code is one worked on at the moment, but as it is not yet giving the expected results improvement of the code is still necessary.

When agreement with the results from the Cargill code is found, a second validation to be done is to compare the results of the iterative process against full 3D methods such as ACTRAN for different geometries. When the method has been properly validated, future work should consist of coupeling the iterative method with for example ATRAN-TM, implementing flow in the equation and demonstrating the effect of the method for realistic duct shapes and frequencies.

11 References

[1] R. J. Astley 2013, personal communication.

[2] A. L. Abrahamson 1977 *American Institute of Aeronautics and Astronautics Paper* 77-1301. A finite element formulation for sound propagation in axisymmetric ducts containing compressible mean flow. (See also NASA CR-145209.)

[3] R. J. Astley and W. Eversman 1978 *Journal of Sound and Vibration* **57**(3), 367-388. A finite element method for transmission in non-uniform ducts without flow: comparison with the method of weighted residuals.

[4] W. Eversman, E. L. Cook, R. J. Beckemeyer 1975 *Journal of Sound and Vibration* **38**(1), 105-123. A method of weighted residuals for the investigation of sound transmission in non-uniform ducts without flow.

[5] P. T. Vo and W. Eversman 1978 *Journal of Sound and Vibration* **56**(2), 243-250. A method of weighted residuals with trigonometric basis functions for sound transmission in circular ducts.

[6] A. McAlpine, M. C. M. Wright, H. Batard and S. Thezelais 2003 *American Institute of Aeronautics and Astronautics Paper* 2003-3305. Finite/boundary element assessment of a turbofan spliced intake liner at supersonic fan operating conditions.

[7] M. C. M. Wright and A. McAlpine 2007 *Journal of Sound and Vibration* **302**, 403-407. Calculation of modes in azimuthally non-uniform lined ducts with uniform flow.

[8] B. J. Tester, C. J. Powles, N. J. Baker and A. J. Kempton 2006 *American Institute of Aeronautics and Astronautics Paper* 44-9. Scattering of sound by liner splices: a Kirchhoff model with numerical verification.

[9] P. Mustafi 2013 *PhD thesis, Institute for Sound and Vibration Research, University of Southampton.* Improved turbofan intake liner design and optimization.

[10] G. Gabard and R. J. Astley 2008 *Journal of Sound and Vibration* **315**, 1103-1124. A computational mode-matching approach for sound propagation in three-dimensional ducts with flow.

[11] B. J. Tester 2013, personal communication.